Behaviour of Helical Pile Groups and Individual Piles under Compressive Loading in a Cohesive Soil

By

Stephen A. Lanyi

A thesis submitted in partial fulfillment of the requirements for the degree of

MASTER OF SCIENCE

in

GEOTECHNICAL ENGINEERING

Department of Civil and Environmental Engineering

University of Alberta
Edmonton, Alberta

Abstract

Helical piles are becoming increasingly common as a result of their wide range of foundation applications. This pile type consists of a steel shaft with one or more helical plates welded near the toe. The axial behaviour of this pile type is difficult to predict because the failure mode is dependent on many factors, including: pile geometry, pile load, soil stiffness, and the degree of installation disturbance. There is a lack of studies that have evaluated helical pile behavior while considering all of these factors. To resist large loads, helical piles are commonly installed in closely spaced groups. However, the engineering behaviour of pile groups, such as their: load-settlement response, installation-induced pore pressure response, effects of soil setup, and failure mode, has not been investigated in current literature.

In the present study, the axial behaviour of single and grouped helical piles under compressive loading was investigated by conducting full-scale field tests at a cohesive soil site in Edmonton, Alberta. The helix-bearing soil layer consisted of a relatively homogeneous glaciolacustrine clay with an undrained shear strength of 65 kPa.

In the first phase of the test program, six single piles, instrumented with strain gauges along the pile shaft, were tested. The inter-helix spacing ratio (s/D) of the piles was varied at 1.5, 3, and 5, where s is the inter-helix spacing and D is the helix diameter. The pile failure mechanism was estimated by comparing the measured load distributions to predicted distributions. The results indicate that at loads below the ultimate state the individual bearing model dominated pile behaviour regardless of the s/D ratio; however, as the pile load increased, significant cylindrical shear resistance might develop. The

bearing capacity factor N_t and the adhesion coefficient α were estimated based on the measured pile component loads and compared to recommended values.

In the second phase, seven 2 × 2 helical pile groups were tested. The pile group spacing ratio (s_g/D) was varied at 2, 3, and 5, where s_g is the center-to-center spacing of piles in a group; the s/D ratio was varied at 3 and 5. The results indicate that group interaction, resulting in a reduction in group performance, increased as the s_g/D ratio decreased and as the group load increased. The group interaction of helical piles was less than that predicted for equally spaced conventional piles. The measured load distributions indicate that individual bearing failure occurred to a grouped pile with an s/D ratio of 5; however, the lower-helix resisted more load than by the upper-helix, compared to a single pile with the same s/D ratio. The measured group capacities and load distributions of the instrumented piles indicated that the grouped piles failed individually, as opposed to as a block.

The effects of soil setup on the behaviour of single and grouped helical piles were evaluated by comparing the load-settlement response of tests occurring 2 to 5 hr after pile installation to comparable tests occurring at least 7 days after installation. Piezometers were installed at the center of selected groups and near a single pile in order to measure the excess pore pressure (u_e) response to pile installation. The results show that u_e significantly reduced the performance of groups; however, the effects of u_e on single piles were limited to the soil very near the pile shaft and did not affect pile performance at the ultimate state. The magnitude of u_e, and the u_e dissipation time, at the center of groups far exceeded that of near a single pile. Also, at the center of groups, the magnitude of u_e increased and the u_e dissipation time decreased as group spacing decreased.

Preface

Chapters 3 and 4 have been submitted to Soils and Foundations and the Canadian Geotechnical Journal, respectively, for possible publication. Although these manuscripts are coauthored by Lijun Deng, the majority of the writing and all the field work and data processing were conducted by myself.

Acknowledgements

I wish to thank and express my gratitude towards my supervisor, Dr. Lijun Deng, for his guidance and support. Throughout this research project Dr. Deng's passion for geotechnical engineering and continued learning helped to motivate and inspire me. I am grateful for the time and hard work that he has devoted to my learning and research.

This research would not have been possible without the financial support of the Natural Sciences and Engineering Research Council of Canada (NSERC), under the Engage Grants program (494853-16) and the financial support of the NSERC–Industrial Postgraduate Scholarship, with the financial contribution from Roterra Piling Ltd. I would also like to thank Roterra for their technical support, including: providing test piles, installing piles, setting up load tests, and providing load test instrumentation. Also, thanks to Moira Guo, Zibo Shen, Chunhui Liu, students at the University of Alberta, for their assistance in laboratory soil testing.

Lastly, I would like to thank my partner, Kelly Bennett, for her love and continual support and encouragement throughout my graduate studies.

Table of Contents

List of Tables

List of Figures

1 Introduction

This chapter contains background information pertaining to helical piles and pile groups, the research objectives, a description of the test program, and the thesis organization.

1.1 Background

1.1.1 Helical Pile General Description

Helical (screw) piles are a deep foundation type consisting of one or more steel helical plates welded at the toe of a hollow cylindrical steel shaft (Figure 1-1). This pile type can be utilized to resist compressive, tensile, and lateral loads. When used to resist tensile loads, a helical pile is usually referred to as an anchor. Helical piles are installed by applying axial force (crowd) and torque to the top of the pile by means of a drive head. A piece of equipment, usually a skid steer or an excavator, is used to hydraulically power the drive head. Figure 1-2 shows a photo of a typical helical pile installation. A helical piling crew typically includes two individuals, an equipment operator, and a swamper. The swamper's job is to assist the equipment operator in positioning the pile and ensuring that the pile is plumb as installation progresses. To reduce soil disturbance, the operator aims to advance the pile one helix pitch per revolution so the helices follow a consistent path as the pile advances (Perko 2009). The torque required to advance the pile into the ground is measured throughout pile installation.

Based on historical load test data, an empirical relationship between installation torque and pile capacity has been developed (Hoyt and Clemence 1989). By applying this relationship, the measured torque can be used as a quality control measure to verify a pile's capacity. During design, a minimum installation torque is calculated to correspond to the pile's design capacity. If the measured torque is below this minimum requirement at its design elevation, extensions may be added to the shaft in order to advance the pile deeper. Extensions are either welded on or attached with a coupling mechanism.

Common applications of this pile type include: underpinning commercial, residential, and industrial buildings; retrofitting existing buildings with failing foundations (Lutenegger 2013); guy-wire anchors used to support power line structures (Perko 2009); and foundations for buildings and bridges in seismic zones (El Naggar and Abdelghany 2007).

Helical piles have various advantages over conventional piles, where the term 'conventional pile' refers to driven or bored piles with a consistent cross-section. These advantages include: high axial capacities compared to equivalent shaft diameter conventional piles, light-weight and mobile installation equipment, minimal soil disturbance caused by pile installation, fast installation time, low noise and vibration during installation, and pile reusability. Additionally, the high uplift resistance of this pile type makes it an excellent foundation options for light-weight structures that are susceptible to frost heave or expansive soils (Perko 2009). Also, helical piles have low down-drag loads compared to conventional piles due to the shaft diameter being smaller than the helix diameter (Carville and Walton 1995).

1.1.2 Load Transfer and Failure Mode of Single Helical Piles

Both theoretical and empirical methods have been developed to estimate the axial capacity of helical piles. The theoretical approach involves the use of equations that are derived from applying static force equilibrium to assumed failure surfaces. To obtain a reasonable capacity estimation, the soil strength parameters and pile failure mode must be known. Improperly characterizing the failure mechanism may result in an overestimation of capacity. The empirical approach to predict pile capacity is based on a relationship between the measured torque required to advance the pile and pile capacity. This torque-capacity relationship is founded on a compilation of load test data that includes a wide range of pile geometries and soil types. The torque-capacity relationship is generally not used for design, as pile installation is required; it is typically only used to verify a piles design capacity when site-specific pile load tests are not performed.

Few of the previous studies investigating the failure mode of helical piles have directly measured the load distribution along the pile. Generally, the failure mechanism has been assumed by comparing the theoretical capacities to measured capacities, or estimated using numerical models. There has been little investigation of the load transfer behaviour of this pile type with the use of strain gauge data. Past studies that have utilized strain-gauge-instrumented piles have mainly focused on the load distribution at pile failure. In addition, the relation between the helical pile geometry and the failure mode seemed inconsistent in the literature. There has also been little investigation of the change in the load transfer as the pile load is increased. For this reason, it may be difficult to predict pile behaviour at serviceability state.

1.1.3 Helical Pile Groups

Helical piles are commonly installed in groups, where pile groups are defined as a collection of closely spaced piles connected at the surface by a pile cap. A pile group may be utilized to resist larger loads than individual piles. Additionally, groups of small diameter piles may be used instead of a larger diameter single pile when it is economocially advantageous to do so because of the lower cost associated with both the fabrication and installation of smaller piles. Site-specific equipment accessibility may also influence the choice to use smaller diameter pile groups. If site-specific constraints were to limit the size of the equipment on site, it may only be possible to install smaller-diameter, shorter piles.

Closely spaced piles will interact due to overlapping stress and strain fields between neighbouring piles. This interaction, known as the group effect, may result in a reduced group capacity and an increased group settlement compared to the capacity and settlement of a comparable single pie under an equivalent load (Meyerhof 1960). Due to the unique geometry of helical piles, the design methodologies used for conventional pile groups may not be applicable for helical pile groups. The group behaviour of this pile type is not well understood as the existing research on this topic is very sparse.

1.2 Research Objectives

The following subsection outlines the objectives of this thesis. These objectives are divided into those related to the behaviour of single helical piles and those related to the behaviour of helical pile groups. The objectives related to the behaviour of single helical piles are to:

- Evaluate the effects of the inter-helix spacing ratio (s/D) on the pile failure mechanism and load transfer behaviour
- Estimate the values of the factors N_t and α; the design factors used in pile capacity estimation in cohesive soil
- Evaluate the effect of installation-induced pore pressure (u_e) generation on short-term pile performance.

The objectives related to the behaviour of helical pile groups are to:

- Evaluate the effects of group pile spacing on group performance
- Determine the effects of group pile spacing on the installation-induced pore pressure (u_e) generation near the piles
- Evaluate the effects of u_e generation on group performance
- Determine the load transfer and the failure mechanism of a pile group.

1.3 Load Test Program

A field load test program was conducted in the fall of 2016 at the University of Alberta farm in Edmonton, Canada. Testing consisted of the axial compressive loading of single helical piles and helical pile groups. All test piles had a length (L) of 6.10 m, a closed-ended shaft of 73-mm-diameter (d), two 305-mm-diamter helices (D), and a helix pitch of 102 mm. Both prior to and during the testing program, a detailed site investigation was performed to determine the physical and mechanical soil properties at this site. Based on the investigation, it was determined that the test piles would be situated below the groundwater table (GWT) within a relatively homogeneous glaciolacustrine clay layer. Selected test piles were instrumented with electrical resistance strain gauges, at four stations along the pile shaft, used to estimate the axial load distribution along these piles. Piezometers were installed at the center of selected pile groups, and near a single pile, used to measure the installation-induced u_e generation and dissipation.

The single pile test program consisted of 6 pile tests with varied inter-helix spacing ratios (s/D = 1.5, 3, 5). All test piles were instrumented with electrical resistance strain gauges. For piles with an s/D ratio of 3, the soil setup time (t_s), or the time between pile installation and load testing, was varied; the piles PA-2 and PA-3 had a t_s of 15 and 12 days, respectively, while PA-4 had a t_s of 2 hours. A piezometer was installed at a radial distance (r) of 450 mm from a selected test pile; the depth of the piezometer was 250 mm above the upper-helix.

The pile group test program consisted of 7 group tests and 4 single pile tests. Single pile tests were required in order to evaluate group performance; the pile group load – settlement curves were compared to those of the single piles. These single pile tests were also analyzed separately under the investigation of single piles behaviour. All pile groups consisted of four piles in a square pattern. The pile group spacing ratios (s_g/D) of these tests were varied at 2, 3, and 5. For groups with an s_g/D ratio of 2 and 3, the soil setup time (t_s) was varied; tests PG-B2 and PG-C2 occurred 5 hr after pile installation, while tests PG-B1 and PG-C1 occurred 8 and 9 days after pile installation. Piezometers were installed at the center of groups PG-B1 and PG-C1 at a depth of 500 mm below the upper-helix. One of the four piles in each of the groups PG-D1 and PG-D2 were instrumented with strain gauges.

1.4 Thesis Organization

This thesis is paper-based and consists of five chapters. Chapter 1 contains an introduction which includes the background information and research objectives and scope. A literature review pertaining to helical piles, pile groups, and pile installation effects are contained in Chapter 2. Chapter 3 contains a manuscript which investigates the behaviour of single helical piles, specifically the progressive development of failure surfaces and the effects of soil setup on pile behaviour. Chapter 4 contains a manuscript which investigates the behaviour and performance of helical piles groups. This includes an investigation of the group performance on the basis of capacity and settlement, the installation-induced pore pressure response in pile groups, the effect of soil setup on group behavior, and the load transfer and group failure mechanism. Chapter 5 contains a summary of the conclusions from this work and recommendations for future research.

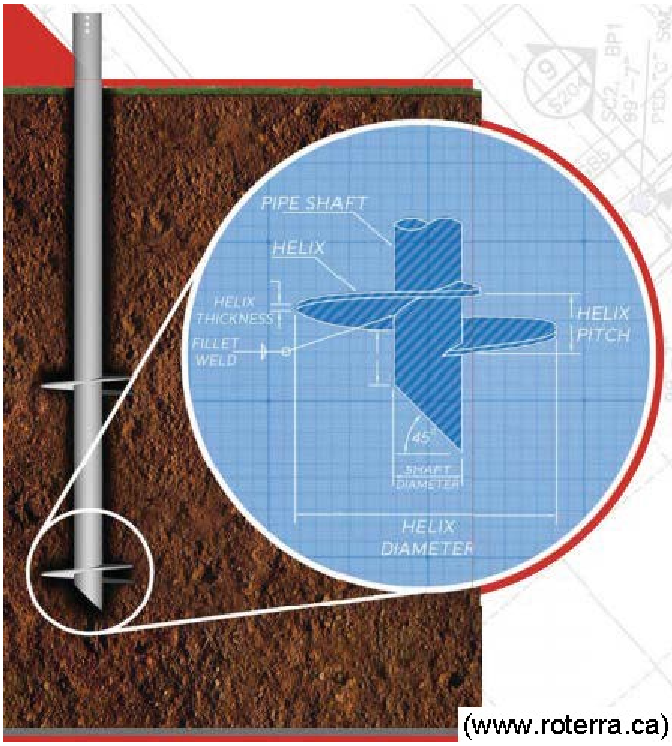

Figure 1-1. Schematic of a typical helical pile.

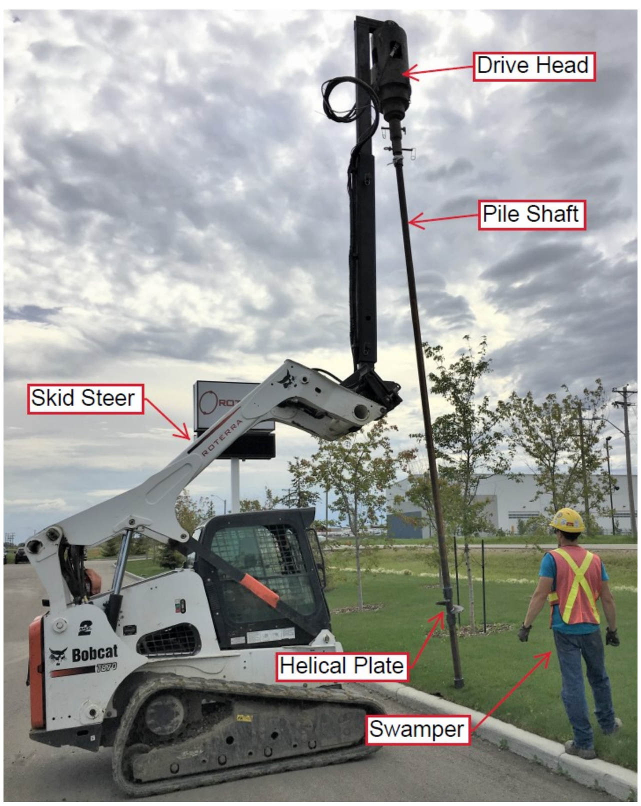

Figure 1-2. Typical helical pile installation.

2 Literature Review

This chapter contains a summary of literature relating to helical piles and piles groups. First, the history of helical piles will be presented, followed by the pile's axial behaviour, including the failure mechanism and capacity prediction. Next, literature pertaining to general pile groups, and specifically helical pile groups, will be presented. Lastly, research on helical pile installation effects will be summarized.

2.1 History of Helical Piles

Helical (screw) piles were invented by Alexander Mitchell in the 19th century. Mitchell first used a helical pile as a mooring to anchor ships at harbor (Lutenegger 2011). Mitchell later expanded upon this idea and designed screw piles to resist structure loads. The first screw piles consisted of an iron helical blade fastened to the end of a slender iron shaft. This pile type was first used in a construction project in 1838 as the foundation for the Maplin Sands Lighthouse (Figure 2-1). Early screw piles were installed by attaching a capstan to the top of the pile shaft. Man or horse power was used to apply torque, screwing the pile into the ground. In the 19th and early 20th century, this foundation type was mainly used for off-shore lighthouses, ocean-front piers, and bridge piers. Helical piles made construction projects possible where they previously were not (Lutenegger 2011). Around 1950 the popularity of this pile type began to grow due to advances in helical pile technology and its installation equipment (Perlow 2011). Today helical piles are used for a wide variety of applications including the foundations for residential, commercial, and industrial structures.

2.2 Axial Compressive Resistance of a Single Pile

The axial load (Q) applied to a single pile is carried in part by the bearing resistance of the pile toe (Q_b) and by the shaft resistance along the surface area of the pile shaft (Q_s). A schematic of the load distribution of a single pile is shown in Figure 2-2. The limit load (i.e. the load causing plunging) for an axially loaded pile is shown in Equation 2-1 (Salgado 2008):

$$Q_L = Q_{bL} + Q_{sL} = q_{bL} A_b + q_{sL} A_s \quad \text{[Equation 2-1]}$$

where q_{bL} is the limit state unit base resistance, A_b is the area of the pile base, q_{sL} is the limit state unit shaft resistance, and A_s is the surface area of the shaft. The following subsection will give a summary of the theory and research related to the end bearing and shaft resistance of piles in cohesive soils.

2.2.1 End Bearing Resistance in Clay

The following derivations and theory are a summary of Salgado (2008). The estimation of the end bearing (toe) resistance of a pile in clay is based on bearing capacity theory developed for shallow foundations (Terzaghi 1943; Meyerhof 1951; Skempton 1951). The value of q_{bL} is determined using the bearing capacity equation (Terzaghi 1943):

$$q_{bL} = cN_c + q_0 N_q + \frac{1}{2}\gamma B N_\gamma \quad \text{[Equation 2-2]}$$

where c is the cohesion, q_0 is the surcharge pressure acting at the base, γ is the soil unit weight, B is the width of the base, and N_c, N_q, and N_γ are bearing capacity factors. End bearing resistance requires large pile displacement to fully mobilizes, as strength is mobilized through shear strain. In undrained condition, the calculation of q_{bL} simplifies to:

$$q_{bL} = 5.14 s_u + q_0 \quad \text{[Equation 2-3]}$$

where s_u is the undrained shear strength. To determine the net bearing resistance available at the pile toe (q_{bL}^{net}), it is common to assume the pressure at the toe due to the weight of the pile is equal to q_0 (Salgado 2008); therefore, the net bearing pressure simplifies to:

$$q_{bL}^{net} = 5.14 s_u \qquad \text{[Equation 2-4]}$$

Shape and depth factors (s_{su} and d_{su}) are added to Equation 2-4 to account for the shape and depth of the toe:

$$q_{bL}^{net} = 5.14 s_{su} d_{su} s_u \qquad \text{[Equation 2-5]}$$

Meyerhof (1951) estimated s_{su} and d_{su} as:

$$s_{su} = 1 + 0.2\frac{B}{L} \qquad \text{[Equation 2-6]}$$

$$d_{su} = 1 + 0.2\frac{D}{B}\text{, for } \frac{D}{B} < 2.5 \qquad \text{[Equation 2-7]}$$

where L is the length of the base and D is the depth of the base. Based on these definitions of s_{su} and d_{su}, q_{bL}^{net} for a pile with a circular shaft is equal to:

$$q_{bL}^{net} = 9.25 s_u \qquad \text{[Equation 2-8]}$$

as s_{su} and d_{su} are equal to 1.2 and 1.5, respectively.

Experimentally, Hu and Randolph (2002) found that the q_{bL}^{net}/s_u ratio of non-displacement piles ranged between 9.3 and 9.9. Salgado (2008) suggests the q_{bL}^{net}/s_u ratio of displacement piles would be higher, and it may be appropriate to use a q_{bL}^{net}/s_u ratio between 10 and 12.

The ultimate bearing resistance ($Q_{b,ult}$) is determined using:

$$Q_{b,ult} = q_{b,ult}^{net} A_b \qquad \text{[Equation 2-9]}$$

where $q_{b,ult}^{net}$ is the net ultimate state unit bearing resistance. For displacement piles in clay the difference between q_{bL}^{net} and $q_{b,ult}^{net}$ should be small (Salgado 2008). The bearing capacity factor N_t is commonly used to determine $q_{b,ult}^{net}$, as:

$$N_t = q_{b,ult}^{net} / s_u$$ [Equation 2-10]

therefore:

$$Q_{b,ult} = N_t s_u A_b$$ [Equation 2-11]

O'Niell and Reese (1999) determined that N_t is dependent on soil stiffness, where N_t increases as s_u increases. A summary of the recommendations of O'Niell and Reese (1999) are shown in Table 2-1. The CFEM (2006) suggests that N_t is dependent on the pile toe diameter (*D*), where N_t increases as *D* decreases. A summary of the CFEM (2006) recommendations are shown in Table 2-2.

2.2.2 Shaft Resistance in Clay

Contrary to end bearing resistance, shaft resistance fully mobilizes with minimal pile displacement (approx. 0.25 to 1% *D*) (Salgado 2008). With continued pile displacement, shaft resistance may decline to a residual value as the soil becomes remolded (Fellenius 1999).

In an undrained condition, q_{sL} is calculated as:

$$q_{sL} = \alpha s_u$$ [Equation 2-12]

where α is the adhesion coefficient. The value of α is difficult to estimate, as it is dependent on the pile type and material, soil type and stress history, degree of soil remolding during pile installation, and the quality of the soil-shaft contact (CFEM 2006).

Several researchers have investigated the correlation between s_u and α. Fleming et al. (2009) suggested that $\alpha > 0.5$ for soft clays and that $\alpha < 0.5$ for very stiff clays. Hu and Randolph (2002) developed an empirical relationship between α and s_u for drilled shaft foundations:

$$\alpha = 0.4\left[1 - 0.12\ln\left(s_u / p_A\right)\right]$$ [Equation 2-13]

where p_A is the atmospheric pressure.

The value of α is also found to depend on the soil stress history (OCR). Randolph and Murphy (1985) developed empirical equations, based on a compilation of load test data on driven piles, relating α to the s_u/σ_v' strength ratio:

$$\alpha = (s_u/\sigma_v')_{nc}^{0.5}\,(s_u/\sigma_v')^{-0.5} \text{ for } s_u/\sigma_v' \le 1 \qquad \text{[Equation 2-14]}$$

$$\alpha = (s_u/\sigma_v')_{nc}^{0.5}\,(s_u/\sigma_v')^{-0.25} \text{ for } s_u/\sigma_v' > 1 \qquad \text{[Equation 2-15]}$$

where σ_v' is the vertical effective stress and the subscript 'nc' refers to the normally consolidated state.

2.3 Load Transfer and Failure Mechanisms

Many researchers have investigated the load transfer behaviour and failure mechanism of helical piles. This literature generally acknowledges two failure models of axially loaded helical piles, the individual bearing model (IBM) and the cylindrical shear model (CSM) (Zhang 1999). Figure 3-1 shows a schematic of these two models. The IBM predicts that bearing failure occurs at each helix and that there is negligible interaction between adjacent helices, while the CSM assumes that soil is trapped between adjacent helices such that a cylindrical shearing surface develops between the upper and lower helices.

Previous research has established that the pile failure mechanism is dependent on the inter-helix spacing ratio (*s/D*), where cylindrical shear failure occurs when *s/D* is small and individual bearing occurs when *s/D* is larger. These studies indicate that the critical *s/D* ratio is between 1.5 and 3. Techniques used to investigate the critical *s/D* ratio include: comparing failure model predicted capacities to measured capacities, estimating the soil-pile interaction using numerical models, and estimating the load distribution using strain gauge data from instrumented test piles.

Rao et al. (1989) and Rao and Prasad (1993) performed model anchor load tests in very soft clay in the laboratory. By comparing the failure model predicted capacities to the measured capacities, they determined that the critical *s/D* ratio was 1.5. Rao et al. (1989) completely removed model anchors from the soil in order to observe the failure surface around the helices. They observed the formation of a soil cylinder for piles with an *s/D* ratio of 1.5 and soil cones, typical of bearing failure, for pile with larger *s/D* ratios.

Tappenden (2007) compiled load test data and performed helical pile field tests from 10 sites across Western Canada. It was determined that using the IBM to predict pile capacity for piles with an *s/D* ratio ≥ 3, and the CSM the *s/D* ratio < 3, resulted in the most reliable estimations of pile capacity.

Lutenegger (2009) performed pullout tests on helical anchors with varied *s/D* ratios in clay. He determined that in cohesive soils there is no district transitional *s/D* ratio between the IBM and CSM, as the critical *s/D* ratio is not only dependent on pile geometry, but also soil stiffness and the degree of soil disturbance cause by pile installation. Also, the load transfer behaviour may change as the pile load increases. At loads below the failure load it was found the individual bearing behaviour occurred, regardless of the *s/D* ratio.

Elsherbiny and El Naggar (2013) performed a study using a finite element model to examine the load transfer behaviour of helical piles under axial loads. It was found that at low loads the IBM dominates pile behaviour regardless of the *s/D* ratio; however, as pile load increases, interaction occurs between the helices occurs and a soil cylinder may develop. Additionally, at smaller *s/D* ratios there is more interaction between helices, and it is more likely the CSM will dominate pile behaviour at high pile loads.

Zhang (1999) investigated the axial behaviour of helical piles by performing field load tests at a cohesive soil site and a sandy soil site. Several test piles were instrumented with strain gauges in order to estimate load distributions along these piles. For piles with *s/D* ratios of 1.5 and 3, significant inter-helix resistance was measured, indicating cylindrical shear behaviour. By comparing the measured pile capacities to the failure model predicted capacities Zhang (1999) found the critical *s/D* ratio to be 3.0 in cohesive soil and 2.0 in cohesionless soil.

Elkasbgy and El Naggar (2015) performed field load tests on strain gauge instrumented helical piles. The test pile helices were located in a layered soil consisting of stiff clay and silty sand. The load distribution data indicated that all piles exhibits individual bearing behaviour, even those with an *s/D* ratio of 1.5. They concluded that the individual bearing behaviour at small *s/D* ratios was caused by installation disturbance softening the soil in the inter-helix region.

2.4 Pile Group Behaviour

2.4.1 General pile groups

When piles are installed in closely spaced groups they may interact when under load. This interaction, known as the group effect, influences the average capacity and settlement of a group compared to that of an equivalent single pile (Poulos 1989). In cohesive soils, group interaction will result in decreased group performance due to overlapping stress and strain field between neighbouring piles, while in cohesionless soils, group interaction may result in improved group performance, as the installation of a pile group may cause an increase in the lateral normal pressure and density of the soil between the piles (Meyerhof 1960). The performance of pile groups can be evaluated on the basis of resistance, by calculating the group efficiency (η_g), or on the basis of settlement, by calculating the settlement ratio (R_s). Refer to Chapter 4 for the definitions of the performance metrics.

Whitaker (1957) performed model pile group tests in clay, varying the number of piles in a group and the spacing between the piles. It was determined that the soil between very closely spaced piles will fail as a block; however, as group pile spacing increases, the failure mechanism transitions, such that the individual piles fail locally. For groups exhibiting local failure, group efficiency decreased gradually with decreased pile spacing; however, for groups exhibiting block failure, group efficiency decreased rapidly with decreased spacing.

Lee and Chung (2005) performed model pile tests in granular soil in order to investigate the favourable interaction that may occur in this soil type. They compared the behaviour of an isolated single pile to that of a single pile installed in the center of a 3×3 pile group. It was determined that installation effects caused densification of the granular soil, causing the single pile installed in the group to have higher shaft and tip resistance compared to that of the single isolated pile.

McCabe and Lehane (2006) performed static load tests on driven precast concrete pile groups in a clayey silt. Groups consisted of four corner piles in a square configuration with one pile in the center. The stiffness of an isolated single pile was compared to that of the center pile in a group loaded alone and to the center pile in a group when all grouped piles were loaded together. The results showed that the load-settlement response of the isolated pile was similar to that of the grouped pile loaded alone; however, when all the grouped piles were loaded, the center grouped pile had a much softer response to loading than the others. These results suggest that installation effects had little influence on group performance, while group interaction during loading significantly reduced group performance.

Mendoza et al. (2015) analyzed the group performance of alluvial anker piles in silty sand using a finite element model. Field tests of pile groups were used to calibrate the model. The results showed that group efficiency was close to unity for all groups tested, indicating minimal group interaction. The estimated soil displacements around the piles suggested that individual pile failure occurred, as opposed to block failure, thus, resulting in negligible group interaction.

2.4.2 Helical Pile groups

There is a very limited set of research pertaining to the performance of helical pile groups. The existing research on this topic is mainly limited to model pile tests and numerical model analysis; however, one study does include the field testing of full-scale helical pile groups.

Trofimenkov and Mariupolskii (1965) performed field pullout tests on groups consisting of three helical piles in a row. The relative spacing between the piles (s_g) varied between 1.5 helix diameters (D) and 5 D. It was determined that for $s_g \geq 1.5D$ there was no resistance reduction for this group geometry.

Ghaly and Hanna (1994) investigated the axial performance of helical anchor groups by performing a parametric load test study on model anchors in sand. Parameters varied included: the number of piles in a group, the group pile spacing, and the sand density. It was concluded that in medium to loose sands the group efficiency increased as anchor spacing increases, while in dense sand, efficiency was greater than 100% at close spacing’s and it decreased with increasing pile spacing. In dense sand, the installation of piles increased the density, resulting in an increase in soil shear strength near the pile

Shaheen and Demars (1995) performed model anchor load tests in a saturated sand. Triangular and row group configurations, with various group pile spacing’s, were tested. They found that in dense sand, group capacity is reduced exponentially with decreased pile spacing, and that at a $s_p \geq 5D$ there is negligible group interaction. In loose sands, it was determined that group performance was independent of group spacing, due to local pile failure.

Livneh and El Naggar (2008) developed a numerical model to evaluate the behaviour of helical piles. The model was calibrated based on the results of field load test performed in a stiff sandy clayey silt. They estimated that for a compressively loaded pile, soil displacement around the helices was negligible at a radial distance of $2D$ from a pile's center. From this, they concluded that adjacent piles spaced further than $4D$ would not interact.

Elsherbiny (2011) performed a parametric study using a finite element model to evaluate the performance of helical pile groups. The parameters varied in this study were: group configuration, group pile spacing, inter-helix spacing, number of piles in each group, and the soil strength parameters. It was determined that in cohesive soils local failure occurred, resulting in less group interaction than for conventional piles. The group performance was found to decline with an increasing number of piles in each group and as group load decreased. Inter-helix spacing was found to have a negligible effect on group performance.

2.5 Effects of Pile Installation

As a helical pile is advanced into the ground, soil is displaced away from the pile shaft and sheared by the helical plates as they cut though the soil. In fine-grained soils, these processes, known as installation disturbance, change the soil stress state near the pile and may alter the soil shear strength (Weech 2002). The change in soil stress is the result of two factors: the increase in total stress, caused by the penetration of the pile shaft forcing soil radially outward from the shaft (Poulos and Davis 1980); and the change in effective stress due to the volumetric response of fine-grained soils to shear strain (Randolph 2003). The increase in total stress will result in positive excess pore pressure (u_e), but a soil's response to shear strain depends on the overconsolidation ratio (OCR) (Weech 2002). Following pile installation, positive excess pore pressure (u_e) generation will result in a reduction in the soil shear strength near the pile, where the reduction in s_u is proportional to the magnitude of excess pore pressure generation (Weech 2002). As u_e dissipates, pile capacity increases proportionally; this phenomena is known as soil setup. The rate of soil setup is directly related to the rate of consolidation near the pile (Soderberg 1962).

Based on cavity expansion theory, Randolph and Wroth (1979) developed an analytical solution for predicting u_e generation around a displacement pile. Following pile installation, they assumed that there would be a region near the pile that would be plastically deformed, as the soil would fail in shear during pile installation. In this region, the instantaneous u_e would be the greatest at the shaft face and u_e would decrease logarithmically with distance from the pile, reaching zero outside the plastic zone. The radius of the plastic zone (R) is given by:

$$R = r_0 \left[G/s_u \right]^{1/2} \qquad \text{[Equation 2-16]}$$

where r_0 is the radius of the pile shaft and G is the soil shear modulus. The value of instantaneous u_e as a function of the radial distance from the pile shaft center (r) is given by:

$$u_e = s_u \left[\ln\left(G/s_u \right) - 2\ln\left(r/r_0 \right) \right] \qquad \text{[Equation 2-17]}$$

In this model, Randolph and Wroth (1979) assumed that cohesive soil is elasto-perfectly plastic and G could be taken as the secant modulus (not G_{max} at small strain) for realistic soil.

Another effect of installation disturbance is soil remolding. Skempton (1950) recognized that the soil traversed by the helices during installation is partially remolded, and proposed the shear strength of the soil mobilized under load should be in between the undisturbed and fully remolded strengths. The degree of soil remolding is difficult to predict since it is largely dependent on the soil type and sensitivity, and the quality of pile installation (Lutenegger et al. 2014).

The effects of installation induced u_e and soil remolding on pile capacity have been investigated by several researchers; however, these studies are mainly limited to conventional piles and have not considered the cumulative effects that occurs in pile groups. A summary of previous research pertaining to the installation effects of helical pile is presented below.

Weech (2002) measured the installation induced pore pressure generation in a soft sensitive clay at various distances away from a pile's shaft. Ultimate capacities were compared for piles load tested 19 hours, 7 days, and 6 weeks after installation. It was found that the majority of the pore pressure generation was due to a total stress increase caused by the penetration of the pile shaft. Excess pore pressure (u_e) was measured up to a radial distance of 60 pile shaft radii from the pile center. Piles with an *s/D* ratio of 3, tested 19 hours after installation, did not have significant capacity reduction compared to equivalent piles tested 6 weeks after installation. Weech proposed this was because the soil mobilized by the helical plates were far enough from the pile that the shear strength was not significantly reduced during pile installation.

Vyazmensky (2005) used the pore pressure data from Weech's study to create a numerical model to predict the pore pressure generation caused by helical pile installation. The NorSand critical state model and Biot's consolidation equations were used for the framework of this finite element model. Cavity expansion theory was implemented to estimate stress changes during pile installation. The numerical model was in agreement with Weech's results, indicating the model could successfully predict u_e generation in soft fine-grained soils.

Lutenegger et al. (2014) quantified helical pile installation-induced soil shear strength reduction by comparing the in-situ undrained shear strength (s_u) of the soil traversed by the helices during installation to the s_u of soil away from the piles. In-situ s_u was measured with a field vane and estimated from CPT data. It was found that pile installation reduced s_u of the soil near the pile shaft, which resulted in a significant reduction in pile capacity. It was proposed that the magnitude of s_u reduction is dependent on the quality of the pile installation and soil sensitivity. A highly sensitive clay would have a greater reduction to s_u, since pile installation causes some degree of soil remolding.

Lutenegger and Tsuha (2015) quantified helical pile installation disturbance by comparing tensile to compressive capacities of equivalent test piles. This was possible because they theorized installation disturbance would further reduce a pile's tensile capacity compared to its compressive capacity. This is because the helices and shaft do not penetrate the soil below the bottom helix, meaning the soil mobilized by the bottom helix, when under compressive loading, will not be remolded. The tensile capacity to compressive capacity ratio was used as an indication of installation disturbance. They determined that the s_u reduction from soil remolding was insignificant in stiff clays; however, the s_u of soft sensitive clays was significantly reduced during pile installation.

Table 2-1. Estimation of N_t based on soil strength (O'Neill and Reese 1999).

Soil Strength	N_t
$s_u \leq$ 50 kPa	6
50 < $s_u \leq$ 100 kPa	8
$s_u >$ 100 kPa	9

Table 2-2. Estimation of N_t based on pile toe diameter (CFEM 2006).

Toe Diameter, D	N_t
$D >$ 1 m	6
0.5 < $D \leq$ 1 m	7
$D \leq$ 0.5 m	9

Figure 2-1. Maplin Sands Lighthouse on a screw pile foundation; constructed in 1838. From Lutenegger (2011).

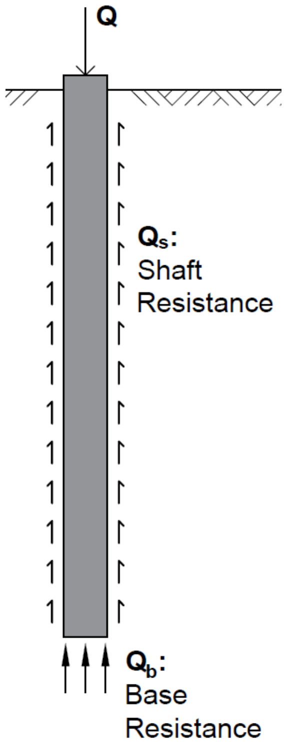

Figure 2-2. Load transfer of an axially loaded pile. After Salgado (2008).

3 Effects of inter-helix spacing and soil setup on the behaviour of axially loaded helical piles in cohesive soil [1]

Abstract

Axial compressive load tests, performed on strain gauge instrumented piles, were completed in order to investigate the effects of inter-helix spacing on the behaviour of helical piles. Test piles had two helices with inter-helix spacing ratios (*s/D*) of 1.5, 3, and 5. The helix-bearing soil layer consisted of a homogeneous clay with an average undrained shear strength of 65 kPa. Test pile failure mechanisms were determined by comparing the measured load distributions to the distributions predicted by the individual bearing and cylindrical shear models. The results indicate that at loads below the ultimate state the individual bearing model dominates pile behaviour; however, as the pile load increases, significant cylindrical shear resistance may develop. The combined bearing capacity factor N_t and the adhesion factor α were evaluated by comparing the measured pile component resistances to theoretical estimations. The back-calculated N_t and α factors were below values traditionally used in helical pile design. The effects of soil setup on pile behaviour were evaluated by comparing the load-settlement response of a pile tested immediately after pile installation to equivalent piles tested many days after installation. A piezometer installed near the upper-helix edge was used to measure the installation-induced excess pore pressure generation and dissipation. The results suggest that the effects of pile installation were limited to the soil very near to the pile shaft and helices and that the soil mobilized during helical plate bearing failure were not significantly softened by the pile installation.

[1] This chapter has been submitted as Lanyi and Deng (2017a) to Soils and Foundations for possible publication.

3.1 Introduction

Helical (screw) piles consist of one or more steel helical plates welded at the toe of a hollow steel shaft. They are installed using mechanical torque and axial force (crowd) applied by a drive head. Common uses of this pile type include: foundations for commercial, residential, and industrial structures; as well as underpinning failing foundations of existing buildings.

3.1.1 Helical Pile Failure Models

Two failure models of axially loaded helical piles are generally acknowledged in literature: the individual bearing model (IBM) and the cylindrical shear model (CSM) (Zhang 1999). Figure 3-1 shows schematics of these failure models. The mechanism of failure is dependent on the ratio of the vertical helix spacing (*s*) to the helix diameter (*D*) (Zhang 1999; Rao and Prasad 1993; Rao et al. 1991). The IBM assumes that the helices are spaced far enough apart such that each helical plate experiences bearing failure and there is no interference between adjacent helices. The CSM assumes that soil is trapped between adjacent helices such that a cylindrical shearing surface develops between the upper and lower helices.

The critical *s/D* ratio, where the transition from the IBM to the CSM occurs, is not definitive in literature. Findings from past studies, which are summarized in Table 3-1, indicate that the critical *s/D* ratio is between 1.5 and 3 in cohesive soils. Lutenegger (2009) concluded that there is no distinct transitional *s/D* ratio between the two models, as the failure mode also depends on the soil type and stiffness. Elsherbiny and El Naggar (2013) determined that at low loads the IBM dominates pile behaviour, even at small *s/D* ratios, but as the pile load increases, the behaviour may transition to the CSM. Most of the preceding studies involving the field testing of instrumented helical piles were conducted in heterogeneous or layered cohesive soils, which may have complicated the evaluation of critical *s/D* ratio. The present study investigates the critical *s/D* ratio, and the transitional behaviour between the IBM and CSM, in a homogeneous cohesive soil.

3.1.2 Compressive Capacity under Undrained Loading

The calculation of the axial capacity of helical piles is derived from applying static force equilibrium to the failure surfaces predicted by the theoretical load transfer models (Figure 3-1). Only the undrained condition in cohesive soil was considered for the present study.

The ultimate compressive resistance (Q_u) of the IBM is estimated by Equation 3-1:

$$Q_u = Q_b + Q_s = N_t s_u A_b N + \alpha s_u \left(\pi d H_{eff}\right) \quad \text{[Equation 3-1]}$$

where Q_b is the bearing resistance of the helical plates, Q_s is the shaft resistance above the upper-helix, N_t is the combined bearing capacity factor, s_u is the undrained shear strength, A_b is the helical plate bearing area, N is the number of helical plates, α is the adhesion factor, d is the shaft diameter, and H_{eff} is the effective shaft length that carries the shaft resistance. H_{eff} is taken as the shaft length above the upper-helix (H_s) minus the length of one helix diameter, which accounts for a void forming above the upper-helix (Elkasabgy and El Naggar 2015).

For the CSM, Q_u is estimated by Equation 3-2:

$$Q_u = Q_b + Q_{cs} + Q_s = N_t s_u A_b + s_u \left(\pi D H_h\right) + \alpha s_u \left(\pi d H_{eff}\right) \quad \text{[Equation 3-2]}$$

where Q_{cs} is the cylindrical shearing resistance of the soil cylinder formed between the helices, Q_b is the helical plate bearing resistance of the bottom helix, and H_h is the shaft length between the top and bottom helices.

The factors N_t and α are required in the computation of Q_u; however, the helical pile specific values of these factors are not well established in the literature. A commonly used value of N_t for helical pile design is 9 (Perko 2009), based on Skempton's experimental work (Skempton 1951); however, Elsherbiny and El Naggar (2013) estimated N_t to be 12 through a finite element analysis, while Zhang (1999) found that an N_t of 9 overestimated the helical plate bearing resistance. Regarding the shaft adhesion, the CFEM (2006) recommends a value of α between 0.5 and 1.0, where α is dependent on s_u, while the ASCE (1993) recommends an estimation for α using the overconsolidation ratio (OCR) and plasticity index (PI). However, Perko (2009) suggests that α is typically lower for helical piles and that shaft adhesion is usually only considered for large-diameter shafts.

An empirical torque-to-capacity relationship is commonly used to predict helical pile capacity, as the measured torque required to advance the pile is an indicator of soil strength at the depth of the helices (Perko 2000). The ultimate pile capacity can be predicted using Equation 3-3 (Hoyt and Clemence 1989):

$$Q_u = K_t \cdot T \qquad \text{[Equation 3-3]}$$

where K_t is the torque correlation factor with units of m^{-1} and T is the final installation torque.

3.1.3 Installation Effects and Soil Setup

During helical pile installation, as the pile advances and the helical plates traverse through the soil, the soil is sheared and displaced outward from the pile shaft. In cohesive soils, this installation disturbance causes destructuring and changes in the soil stress state, resulting in a pore pressure response near the pile (Weech 2002). In normally consolidated to lightly overconsolidated soils the pore pressure response is positive, causing a shear strength reduction. This positive excess pore pressure (u_e) generation can be attributed to two factors: the increase in mean total stress caused by the radial soil deformation outward from the pile shaft (Poulos and Davis 1980) and the contractant shearing response of this soil type (Randolph 2003). The magnitude of u_e near the pile is dependent on soil type, OCR, degree of fissuring, and hydraulic conductivity (Simonsen and Sorensen 2016). Weech (2002) measured u_e at various distances away from the helix edge in a sensitive clay using piezometers, and Lutenegger et al. (2014) quantified the reduction in s_u caused by pile installation by measuring in-situ shear strengths near the helical plates of an installed pile.

Soil setup, or the increase in pile capacity with time, is directly related to consolidation and the dissipation of u_e near the pile (Soderberg 1962). The effects of soil setup on the behaviour helical piles is not well understood. This is because of the limited number of studies that have measured installation-induced u_e and compared pile capacities at different setup times.

3.2 Research Objectives and Scope

The present study examines the behaviour of helical piles under axial compressive loading in a homogeneous cohesive soil. Six load tests of double-helix circular-shafted piles were performed at a test site at the University of Alberta Farm in Edmonton, Canada. The objectives of this study are to: (i) evaluate the effects of the *s/D* ratio on the pile failure mechanisms and load transfer behaviour; (ii) estimate the values of the factors N_t and α for helical piles; and (iii) evaluate the effects of soil setup on pile behaviour.

Test piles were instrumented with strain gauges that were used to estimate the axial load distribution along the pile shaft. All test piles were 6.10 m long with a shaft diameter of 73 mm and a helix diameter of 305 mm. Test piles were designed with inter-helix spacing ratios of 1.5, 3, and 5. A comprehensive site investigation consisting of in-situ and laboratory testing was conducted to determine the cohesive soil's physical, mechanical, and hydraulic properties. The test pile helices were located below the groundwater table (GWT) within a homogeneous, lightly-overconsolidated stiff clay layer.

The measured load distributions, derived from the strain gauge data, were compared to the predicted distributions of the theoretical failure models. The helical bearing resistance (Q_b) and shaft resistance (Q_s), determined from the measured load distributions, were used to estimate the values of N_t and α respectively. To evaluate the effects of soil setup on pile behaviour, the load versus settlement response of a pile tested two hours after pile installation was compared to piles tested many days after pile installation. A piezometer was used to measure the u_e generation and dissipation near the helix edge of a test pile.

3.3 Test Site and Investigation

The test site was located at the University of Alberta Farm in Edmonton, Canada. The subsoils at this location represent a typical soil profile of the Edmonton area. The surficial geology at this site is the result of the formation of Glacial Lake Edmonton during the Wisconsin glacial period, some 12 000 years ago (Godfrey 1993). Prior to, and during the load testing program, a detailed site investigation was conducted. The investigation included cone penetration testing (CPT), Shelby tube sampling, and piezometer installation. Figure 3-2 shows the location of the site investigation activities relative to the test pile locations. Laboratory soil characterization, consolidation, and strength testing were performed on soil samples retrieved from the Shelby tubes.

The soil stratigraphy was interpreted using a combination of the CPT data, lab testing, previous knowledge of the site geology (Bayrock and Hughes 1962), and a review of past site investigations performed near this site (Zhang 1999; Tappenden 2007). Figure 3-3 shows the soil stratigraphy profile, a summary of the soil characterization results, the variation of the GWT depth during the testing program (Oct. to Dec. 2016), the CPT cone tip resistance and sleeve friction profiles, and the variation of undrained shear strength (s_u) with depth. The stratigraphy profile suggests that the top 0.7 m consists of topsoil underlain by a 0.8 m desiccated clayey silt crust (MH). Below a depth of 1.5 m, there exists a 4.5 m thick uniform stiff glaciolacustrine clay layer (CH) underlain by a 1.5 m thick layer of interbedded silty clay (CL) with sand seams. At a depth of 7.5 m there is a 2 m thick silty sand deposit, interbedded with silty clay; this layer is underlain by till at an approximate depth of 9.5 m

Laboratory soil classification, including Atterberg limits, moisture content, bulk unit weight (γ_b), and specific gravity of solids (G_s) testing, were conducted on soils from Shelby tubes from boreholes BH-1 to BH-4 from depths between 0.75 and 6.55 m. Consolidation testing was performed on the soils from BH-5 at depths of 4.72 and 5.33 m. The soil unit of the most importance to the present study was the saturated glaciolacustrine clay (CH), as the majority of the test pile, including the helices, were situated in this layer. The properties of the saturated glaciolacustrine clay are as follows: γ_{sat} of 18.1 kN/m^3, G_s of 2.74, void ratio of 1.02, and a moisture content of 37.4%. The clay has a sensitivity range of 1.0 to 1.6, estimated by the ratio of s_u to the sleeve friction f_s (Robertson and Cabal 2015). The plasticity index and liquid limits indicate that the clay has a USCS classification 'CH', or a fat clay. From consolidation test data, the OCR was found to range between 1.1 and 1.5, while the vertical hydraulic conductivity (k_v) was approximated as 1x10^{-10} m/s. The GWT depth varied from 3 m deep in October 2016 to 4 m deep in December 2016 (Figure 3-3).

The s_u of soils from Shelby tubes were measured in the lab by performing unconfined compressive strength (UCS) testing. The s_u was also estimated from the CPT cone tip resistance using Equation 3-4 (Robertson and Cabal 2015):

$$s_u = \frac{q_t - \sigma_v}{N_{kt}} \qquad \text{[Equation 3-4]}$$

where q_t is the corrected cone tip resistance, σ_v is the overburden stress, and N_{kt} is an empirical factor ranging from 10 to 18. Based on a previous site investigation near the test site (Tappenden 2007) an N_{kt} value of 18 was used. The lab measured s_u of the saturated stiff clay varied between

53 and 95 kPa, while s_u estimated from the cone resistance data varied between 55 and 95 kPa. Figure 3-3 also shows the averaged s_u profile, which will be used in the subsequent analysis of the pile load transfer.

3.4 Load Test Program

The load test program consisted of six axial compression load tests on double-helix piles with varied inter-helix spacing ratios (s/D). Testing was conducted from October to December 2016. Test piles were instrumented with strain gauges at four stations along the pile shaft. For a test pile with an s/D ratio of 3, a piezometer was used to measure the installation-induced u_e generation and dissipation.

3.4.1 Test Piles and Instrumentation

Six double-helix test piles were manufactured, installed, and tested. Table 3-2 shows a summary of test pile geometries. Test piles were 6.10 m long, with a shaft diameter (d) of 73 mm, a helix diameter (D) of 305 mm, and a helix pitch of 102 mm. The shafts were closed-ended to prevent soil from entering the shaft and damaging the strain gauge wiring. Three inter-helix spacing's were used, with s/D ratios of 1.5, 3, and 5. For a set of pile tests (PA-2, PA-3, PA-4) with equal inter-helix spacing ratios ($s/D = 3$) the soil setup time (t_s), or the time between pile installation and load testing, was varied; PA-2 and PA-3 had a t_s of 15 and 12 days, while PA-4 had a t_s of 2 hours.

All test piles were instrumented with electrical resistance strain gauges at four stations along the pile shaft. A Wheatstone full-bridge circuit was used at each station. Figure 3-4 shows the location of each strain gauge station (SG-1 to SG-4) on a test pile. This gauge configuration was chosen so the differential load measured between adjacent SG stations could resolve the load resisted by each major pile component (upper-shaft, upper-helix, inter-helix, lower-helix).

An epoxy and a water-resistant coating were applied to the gauges to prevent damage. Steel covers were manufactured and installed over the gauges to protect them during installation (Figure 3-5). The covers consisted of two hollow half-cylinder steel pieces that fit together to form a continuous steel barrier around the shaft at the gauge locations. The covers were approximately 100 mm in length with a thickness of 15 mm. To fasten the covers to the shaft a threaded rod ran through the cover and the shaft, through drill holes, and was bolted at both ends. Since the covers were bolted to the shaft, they did not change axial stiffness of the shaft.

3.4.2 Piezometers

For test PA-1 a drive-point vibrating wire piezometer was used to measure the u_e generation resulting from the pile installation. Three other piezometers, installed on site for a concurrent testing program, were used to determine the GWT depth throughout the current testing program. Figure 3-2 shows the locations of the piezometers in relation to the test piles.

The piezometers consisted of a 25 mm diameter shaft with a coned tip that housed the vibrating wire diaphragm. An adaptor was used to screw the shaft onto a 51 mm diameter section of drill rod. Coupling pieces were added to extend the piezometer assembly to the length required. Before piezometer installation a 150 mm diameter borehole was drilled with an auger at a radial distance (r) of 450 mm from the planned location of PA-1, to a depth of 3.5 m. The borehole was cased with a 114 mm diameter steel pipe to prevent sloughing into the hole. The piezometer was then placed into the hole and pushed the remaining 1 m to the target depth that was 250 mm above the upper-helix of PA-1. This depth was chosen so the pore pressure near the helical plates could be measured. It was expected that a maximum pore pressure response would occur above the helices because the most soil disturbance would occur here, as both helices would pass this location as the pile is installed. Figure 3-6 shows a schematic of the piezometer installation for PA-1. Piezometer readings were stored once every 2-minutes using a datalogger.

3.4.3 Load Test Setup

Figure 3-2 shows the test pile and reaction pile layout in relation to the site investigation activities. Reaction piles were spaced 5.8 m apart and test piles were spaced 1.52 m apart (2.14 m from the closest reaction pile). With this configuration, the minimum center-to-center spacing between adjacent piles was five helix diameters of the larger pile.

Figure 3-6 shows a schematic of the load test setup and Figure 3-7 shows a photo of a typical setup. This setup consisted of a reaction beam supported by two reaction piles. The reaction piles were 6.1 m long, with a shaft diameter of 140 mm and three 457 mm diameter helices spaced with an *s/D* ratio of 3. No axial displacement of the reaction piles was observed during pile loading tests. A 7 m long, W 840 x 299, I-beam was used as the reaction beam. This beam was fastened to the reaction piles using two 25 mm diameter threaded rods slotted through two 51 mm thick steel plates. A hydraulic jack was used to apply the load to the test piles while a strain gauge load cell was used to measure the load. Pile settlement was measured using two linear potentiometers (LPs) fastened to either side of the loading plate. The load cell and LPs were calibrated prior to the testing program. The installation torque was recorded manually at a 0.3 m interval.

When a helical pile is loaded to near its ultimate capacity it may rotate due to the pitch of the helical plates. Rotation will reduce a pile's ultimate capacity since rotation becoming the limiting state over typical bearing failure. In practice, pile rotation is usually not possible because the pile cap is fixed to the superstructure. For this testing program, the pile rotation was prevented to simulate a practical loading scenario. To provide a moment to resist pile rotation a collared loading plate with hooked ends was placed over the test pile and bolted on. A chain was then wrapped around the nearest reaction pile and looped around the hooked end of the loading plate, and tightened with chain-tensioning tool (Figure 3-7). Because no measures were taken to prevent pile rotation for the first test, PA-1, the load-settlement response of this pile was not appropriate for the analysis of the pile performance; nevertheless, the piezometer record near PA-1 was useful for investigating the pore pressure response caused by pile installation.

3.4.4 Test Procedure

All pile load testing followed the ASTM (2007) "quick test" axial compression load test procedure (D1143/D1143M – 07). The applied load was increased in increments of approximately 5% of the design load. In each increment, the load was held until the rate of axial pile displacement approached zero. A constant time interval of five minutes between loading increments was used. Piles were loaded until plunging failure, or until additional settlement resulted in no further increase in pile resistance. After reaching a maximum load, unloading occurred in five approximately equal decrements. The measurements were recorded using a datalogger at a 0.2-Hz sampling frequency.

3.5 Results and Discussion

3.5.1 Selection of Failure Criterion

In pile testing, failure is often defined as the load causing additional pile settlement with no further increase in pile resistance (known as plunging failure). Equipment limitations associated with load tests often prohibit reaching this load. For this reason, ultimate load criteria have been developed that are based on the shape of the load-settlement curve (Livneh and El Naggar 2008). Figure 3-8 shows the pile head load versus the axial settlement of test piles. As the test piles were incrementally loaded they exhibited three distinct behaviours, characterized by: an initial linear elastic region, a non-linear region at the on-set of plastic soil deformation, and a linear failure region of low stiffness. In the linear failure region, the creep settlement was high, leading to a difficulty in maintaining a constant load. Elkasabgy and El Naggar (2015) suggested that to reduce load test error the ultimate load should fall within the non-linear region, where the creep settlement is much less. Based on this recommendation, and a study of the load-settlement curves (Figure 3-8), the ultimate load criterion adopted for this study was the load causing pile settlement of 5% of the helix diameter, or 15.2 mm. Table 3-2 shows a summary of the load test results including the ultimate capacity (Q_u), final installation torque (T), and torque correlation factor (K_t).

3.5.2 Load Transfer and Failure Mechanism

The differential strain measured between adjacent strain gauge stations was used to determine the load carried by the main pile components: the upper-shaft, upper-helix, inter-helix, and lower-helix. The test pile failure mechanisms were determined by comparing the measured load distributions to IBM– and CSM–predicted distributions that were calculated using Equations 3-1 and 3-2. The parameters used in predicted distribution calculations were: α of 0.5, N_t of 9, and s_u from the profile in Figure 3-3. The load distributions of PB-1, PC-1, PA-2, and PA-3 and the IBM– and CSM–predicted distributions are shown in Figures 3-9a to 3-12a. The test pile distributions are plotted at several load increments to show how the load transfer mechanism progresses throughout the load tests. Figures 3-9b to 3-12b show the pile component loads plotted against pile settlement (S). These plots show how the load resisted by the major pile components develop throughout the load tests. Complete data sets from all four strain gauge stations were obtained from PA-2, PA-3, and PC-1, while the remaining piles had at least one strain gauge station with a noisy signal, perhaps due to a loose electrical connection. The noisy data could not be used for load distribution analysis; however, the reliable data from these piles could still be used to partially resolve their load distributions and component loads.

Figure 3-9 shows the load distribution of PB-1 (s/D = 1.5). For this pile only the upper three strain gauge stations produced high-quality data, which meant that only the shaft resistance (Q_s) and upper-helix resistance (Q_{b1}) could be resolved. Figure 3-9a shows that the IBM prediction of Q_{b1} was close to the measured resistance. Figure 3-9b shows that Q_{b1} increased throughout the load test. The maximum value of Q_{b1} was exactly equal to the IBM predicted resistance. Based on the findings from the other instrumented piles, the lower-helix resistance is likely similar to that of the upper-helix, indicating that significant inter-helix resistance (Q_{cs}) could not have developed.

For test PC-1 (s/D ratio of 5), Figure 3-10a shows that the measured load distribution closely matches the IBM–predicted distribution. Figure 3-10b shows that significant bearing resistance developed for both helices; however, Q_{b1} was slightly less than Q_{b2}. This difference can be attributed to the larger bearing surface of the lower-helix, which includes the shaft tip. The inter-helix resistance (Q_{ih}) increased throughout the load test to a maximum of 17 kN (Figure 3-10b); this corresponded to 18% of the CSM–predicted Q_{ih}.

The load distribution data from PA-2 and PA-3 (s/D ratio of 3, Figures 3-11 and 3-12) show that, at Q_u, the IBM better predicts the pile behaviour than the CSM. This is shown by upper and lower helices carrying similar and substantial resistances, while the inter-helix resistance (Q_{ih}) was considerably smaller than the CSM prediction. Another interesting observation is that Q_{ih} increased as the piles were loaded past the ultimate state to plunging failure, as indicated by the differential load between SG-3 and SG-4. For PA-2 the increase in Q_{ih} was small (Figure 3-11b), at approximately 5 kN; for PA-3 the increase in Q_{ih} was significant (Figure 3-12b), at approximately 20 kN. Beyond the ultimate state, Q_{ih} of PA-3 was better predicted by the CSM, as significant cylindrical shear resistance had developed.

The measured Q_{ih} for PA-2 and PA-3 indicate that neither the IBM nor the CSM accurately predicted the load resisted in the inter-helix region beyond the ultimate state. The trend of Q_{ih} of pile PA-3 especially, showed that the development of a soil cylinder and cylindrical shearing resistance was progressive, while the upper-helix still carried a significant load. Figure 3-13 shows the postulated behaviour of soil cylinder development for PA-3 at three different stages of its loading test. The three stages, corresponding to those in Figure 3-12b, were: 1) in the linear elastic region, 2) near the ultimate load, and 3) at the maximum load where the pile plunged.

At Stage 1 (Figure 3-13a), a partial soil cylinder has developed under the upper-helix. Below the cylinder a rigid cone forms, typical of bearing capacity failure. The soil adjacent to the cone plastically flows along a concave slip-surface, mobilizing shear resistance that contributes to Q_{b1}. Shearing along the cylinder and the vertical component of the shear along the cone contribute to the inter-helix resistance (Q_{ih}); the shaft resistance in the inter-helix region is assumed zero, because the effective length is likely negligible. Bearing failure slip-surfaces also develop under the lower-helix.

At Stage 2 (Figure 3-13b), Q_{ih} increases from Stage 1 as the soil cylinder further develops under the upper-helix, causing the soil cone to form deeper. Q_{b1} and Q_{b2} also increase, as more soil plastically deforms around the helices, causing more resistance to be mobilized along the slip-surfaces. Q_{b2} exceeds Q_{b1} as the bearing area of the lower-helix includes the shaft tip.

At Stage 3 (Figure 3-13c), Q_{ih} reaches a maximum as the soil cylinder has further developed. The bearing resistance of the upper-helix declines as interaction between the helices occurs. The mobilization of shear resistance of the upper-helix is partially obstructed by the lower-helix. The bearing resistance of the lower-helix is unchanged from Stage 2.

The magnitude of Q_{ih} can be used to infer the length of the soil cylinder formed between the helices. By assuming the measured Q_{ih} is equal to Q_{cs}, we used Equation 3-2 to back-calculate the length of the cylinder from the measured Q_{ih}. Figure 3-14 shows the estimated soil cylinder lengths (H_c) plotted against the pile load (Q). At the maximum pile loads, H_c for PA-2 was 325 mm, while for PA-3 it was 635 mm. This difference is likely due to the shear strength of the soil in the inter-helix zone. The final installation torque (T) was used to compare the shear strength of the localized soil in contact with the helical plates between test piles. The final installation torque of PA-3 was 3.73 kN*m, less than 4.34 kN*m for PA-2; indicating the shear strength in the inter-helix zone was weaker for PA-3. Since the shear strength was weaker, it may have been easier for a cylindrical shear surface to develop, because the force required to mobilize shearing across the cylindrical surface would have been less.

3.5.3 Helical Plate Bearing Resistance

To evaluate the helical plate bearing resistance, the ratio of the unit bearing resistance to the undrained shear strength (q_b/s_u) was calculated; where the unit plate bearing resistance (q_b) equals Q_b divided by the plate bearing area (A_b). Figure 3-15 shows the q_b/s_u ratio versus pile settlement. At the ultimate load, the measured q_b/s_u ratio should be equivalent to the combined bearing capacity factor N_t, defined as:

$$N_t = \frac{q_{b,ult}}{s_u} \quad \text{[Equation 3-5]}$$

where $q_{b,ult}$ is the unit bearing resistance occurring at Q_u. Figure 3-15 shows that it takes approximately 15 to 20 mm of settlement (5% to 6.5% D) to fully mobilize the helical plate bearing resistance. At Q_u, q_b/s_u was relatively consistent between the upper and lower helices, ranging between 6.2 and 7.7. As the piles were loaded to plunging failure, q_b/s_u of the upper-helix varied between 4.9 and 9.0, while for the lower-helix the q_b/s_u ratio ranged between 6.6 and 7.5. The low values at pile plunging for the upper-helix might be caused by the bearing resistance of the upper-helix being reduced by the interaction with the lower-helix. At and beyond Q_u, the measured q_b/s_u ratio was less than 9.0 for all piles except for PB-1. This implies that using an N_t of 9.0, a common value used for N_t (Perko 2009), would have resulted in an overestimation of helical plate bearing resistance.

The low values of the measured q_b/s_u ratio at failure may be caused by the shape of the helical plate and soil remolding during pile installation. By using an $\mathrm{N_t}$ value of 9.0, the bearing area is assumed parallel to the ground surface (Skempton 1951); however, the bearing surface of a helical plate is inclined due to its pitch. Vesic (1973) showed that the base inclination of a bearing surface will reduce its ultimate bearing resistance. A reduction in s_u caused by soil remolding during pile installation may have also lowered the q_b/s_u ratio. Skempton (1950) found that soil is remolded by the passage of the helical plates during pile installation. He proposed that the average mobilized shear strength of the helical plates is in between the undisturbed and fully remolded shear strengths. The degree of soil remolding near the lower-helix should be lower than near the upper-helix, as the helices do not pass through much of the soil that was mobilized by the lower-helix. This is consistent with the findings of the present study, as on average the q_b/s_u ratio of the lower helices were higher than the upper helices.

3.5.4 Shaft Adhesion

The measured shaft resistance (Q_s) was used to evaluate the shaft adhesion throughout the loading tests. Equation 3-6 was used to calculate the mobilized shaft adhesion factor α:

$$\alpha = \frac{Q_s}{s_u \cdot (\pi d H_{eff})}$$ [Equation 3-6]

where s_u was interpreted from the CPT and UCS test results (Figure 3-3). Figure 3-16 shows the mobilized α factor versus pile settlement for all tests. PA-1, PA-3, and PB-1 exhibited similar behaviour, where the shaft adhesion reached a peak value at a settlement between 3% and 5.5% of the shaft diameter. The peak α values of these tests were between 0.11 and 0.14. Following the peak, the shaft resistance declined. This decline can be attributed to strain softening behaviour resulting in the strength of the soil adjacent to the shaft trending to a residual value with increased shear strain (Fellenius 1999). PA-2 and PC-1 did not exhibit a peak and post-peak strain softening behaviour as the other piles did. For these tests, the shaft resistance increased with pile settlement, plateauing as the piles approached plunging failure. The maximum α values were 0.29 for PA-2 and 0.26 for PC-1.

At the ultimate load, the measured shaft adhesion factors ranged between 0.06 and 0.29. These are below the values recommended by ASCE (1993) and CFEM (2006). The low shaft adhesion may have been caused by wobbling during pile installation, inhibiting soil-shaft contact (Perko 2009).

3.5.5 Effects of Soil Setup on Pile Behaviour

The load-settlement behaviour of PA-4, with a t_s of two hours, was compared to piles with a t_s of 15 days (PA-2) and 12 days (PA-3). Based on the observations from Weech (2002), it was expected that u_e would be near a maximum at the time of testing PA-4, while u_e was expected to have dissipated at the time of testing PA-2 and PA-3. To support this claim, the installation-induced u_e was measured for a comparable pile, PA-1, using a piezometer. The piezometer was installed at a radial distance (r) of 450 mm from the pile center and a vertical distance of 250 mm above the upper-helix (Figure 3-17b). It was appropriate to use the piezometer data from PA-1 to interpret the behaviour of PA-2, PA-3, and PA-4 because the site was considered homogenous and the pile geometry and embedment depth were consistent for all piles.

Figure 3-17 shows the measured u_e normalized by the initial vertical effective stress (σ'_{v0}) plotted versus the time after PA-1 installation. The peak u_e/σ'_0 ratio was 0.0255 (u_e = 1.85 kPa), occurring 22 hours after pile installation. The time-lag between pile installation and measuring the peak u_e is the result of a redistribution of pore pressure caused by a hydraulic gradient between the soil adjacent to the pile and the soil near the piezometer (Sully and Campanella 1994). The hydraulic gradient between the pile and piezometer is caused by a radial distribution of u_e, such that the magnitude of u_e increases closer to the pile (Weech 2002). For PA-1, the low peak u_e/σ'_{v0} is likely due to the distance between the piezometer and the pile shaft (r/r_s = 12.3 where r_s is the shaft radius, Figure 3-17). The low peak u_e/σ'_{v0} suggests that the shear strength reduction due to pile installation at the piezometer location was negligible. Figure 3-17a shows that u_e was completely dissipated at 5 days after the pile installation; this implies that u_e dissipation was also complete at the t_s of PA-2 and PA-3.

The effect of pile-installation-induced u_e on pile behaviour was investigated by comparing the load-settlement curves of PA-4 to PA-2 and PA-3. Because these piles had varied t_s and different installation torques (Table 3-2), it was not appropriate to compare their measured load-settlement responses directly. We therefore plotted the normalized loads versus the pile settlements (Figure 3-18). For tests with complete u_e dissipation (PA-2 and PA-3), the pile load was normalized by the measured Q_u, defined in the preceding section. For PA-4, the pile load was normalized by the expected Q_u if complete u_e dissipation would have occurred. This expected Q_u was estimated using the capacity-torque relationship (Equation 3-3), where the torque-capacity factor (K_t) used was an average between the measured K_t from tests PA-2 and PA-3 (or 23.65 m^{-1}, Table 3-2).

A comparison of the Q/Q_u – settlement plots (Figure 3-18) shows that, at loads below Q_u, PA-4 exhibited a softer response to loading than PA-2 and PA-3. At loads beyond Q_u, the three curves read almost the same. To quantify the variation in the Q/Q_u – settlement behaviour between these piles, the resistance ratio (R_r) was calculated, where we define R_r as:

$$R_r = \frac{Q_{u_e}^N}{Q_{u_0}^N} \qquad \text{[Equation 3-7]}$$

where $Q_{u_e}^N$ is the normalized load before the complete u_e dissipation and $Q_{u_0}^N$ is normalized load after the complete u_e dissipation, calculated at equal pile settlement. $Q_{u_e}^N$ was determined from the Q/Q_u – settlement curve of PA-4, while $Q_{u_0}^N$ was determined from the average of the Q/Q_u – settlement curves of PA-2 and PA-3.

Figure 3-19 shows the R_r versus settlement plot for PA-4 with respect to PA-2 and PA-3. This plot shows that R_r was a minimum value (0.75) at the beginning of the load test. As the pile settlement increased, the resistance ratio approached unity, indicating the resistance of pile PA-4 was equal to that of an equivalent pile with complete u_e dissipation. As pile settlement exceeded 15 mm, and approached plunging failure, R_r was relatively constant ranging from 1.0 to 1.04.

The measured u_e near PA-1 was used to interpret the R_r trend of PA-4. The magnitude of the measured u_e near-PA-1 was an indicator of the degree of soil strength reduction near PA-4. At low pile settlement, the soil mobilized by the helical plates was close to the pile, causing R_r to be low (Figure 3-19). When testing of PA-4 began, at a t_s of 2 hours, u_e near to the pile shaft and helix should have been near a maximum. This means the soil shear strength near the pile was lower than that of the comparable piles, PA-2 and PA-3, where u_e was zero at the beginning of pile testing. As PA-4 settled further, R_r increased because the bearing failure of the helical plates mobilized soils further from the pile. From finite element analyses, Elsherbiny (2011) showed that in clay, with an s_u between 50 and 100 kPa, soil was mobilized to a radial distance of 2.6 times the helix radius. Therefore, the soil in the present study would likely have been mobilized at a maximum radial distance of approximately 400 mm away from the center of the pile. Figure 3-17 shows that at the time of PA-4 testing (t_s = 2 hours), the u_e at an r of 450 mm was negligible (u_e/σ'_{v0} = 0.005). The R_r of PA-4 approaching unity with increased settlement, and the low u_e measured away from PA-1, indicate that the reduction in shear strength to the soils mobilized by the helical plates must have been negligible. This observation is consistent with Weech and Howie (2012) that found no pile-installation-induced strength reduction to the soil mobilized by helical piles exhibiting individual bearing failure.

3.6 Conclusions

Field load tests were conducted on six helical piles at a cohesive soil site. The inter-helix spacing ratios (*s/D*) of these piles were 1.5, 3, and 5. Three identical piles with an *s/D* of 3 were tested at various soil setup times after the pile installation. The following conclusions may be drawn:

1. In the homogeneous stiff cohesive soil (s_u = 65 kPa), the individual bearing model dominated pile behaviour at the ultimate state. Piles with *s/D* ratios of 1.5, 3, and 5 had measured cylindrical shear resistances far below the cylindrical shear model predicted resistance and had helix bearing resistances closely predicted by the individual bearing model.
2. A model is proposed to describe the transition from individual bearing behaviour to cylindrical shear behaviour. This process involves the progressive growth of a soil cylinder under the upper-helix. As the pile load increases the soil cylinder extends toward the lower-

helix. The bearing resistance of the upper-helix begins to decline when the lower-helix begins to obstruct the mobilized shear resistance of the upper-helix bearing.

3. Helical pile load transfer behaviour in cohesive soils is not only dependent on the inter-helix spacing ratio, but also the soil strength and pile load. It is more likely for a larger soil cylinder to develop, and the cylindrical shear model to dominate pile behaviour, in less stiff soils. This is because less force is required to mobilize shearing along the cylindrical surface.
4. The measured bearing capacity coefficient (N_t) for the helical plates was between 6.2 and 7.7 at the ultimate pile load, substantially below the commonly used value of 9. The low measured N_t values are likely due to the inclination of the helical plate bearing surface. Helical plate bearing resistance was found to fully mobilize after a pile settlement of 15 to 20 mm (5% to 6.6%D).
5. The measured shaft resistance (Q_s) of most the test piles reached a peak after 2 to 4 mm (3% to 5.5%d) of pile settlement. The peak shaft adhesion factors (α) of these piles were between 0.11 and 0.14. At plunging failure, the measured α of these piles were between 0.06 and 0.10.
6. Installation-induced u_e caused a temporary resistance reduction to a pile tested 2 hours after installation (PA-4). At low settlement, the resistance ratio (R_r) of PA-4 with respect to PA-2 and PA-3 was 0.75; however, as the pile was loaded to its ultimate capacity, R_r approached unity. The increased settlement caused the bearing failure of the helical plates to mobilize soil shear resistance further from the pile where u_e generation was negligible.

Table 3-1. Summary of past research regarding the critical *s/D* ratio in cohesive soils.

Source	Critical *s/D* Ratio[a]	Soil Type	Test Method	Analysis Method
CFEM (2006)	3	N/A	N/A	N/A
Elkasabgy and El Naggar (2015)	<1.5 [b]	Silty clay (s_u = 85 kPa), overlying very stiff clay (s_u = 137 kPa), clay till (s_u = 177 kPa)	Field test	Strain gauge data
Rao et al. (1989)	1.5	Very soft clay, s_u = 2 – 9 kPa	Small-scale lab test	Back-calculation, observation
Rao et al. (1993)	1.5 to 2.0	Marine clay, s_u = 3 – 8 kPa	Small-scale lab test	Back-calculation
Rao and Prasad (1993)	1.5	Marine clay, s_u = 3 – 8 kPa	Small-scale lab test	Back-calculation
(Tappenden 2007)	3	Many test sites: silt, clay, till	Field test	Back-calculation
Tappenden et al. (2009)	1.5	Stiff clay, s_u = 50 – 100 kPa	Field test	Strain gauge data
Zhang (1999)	3	Stiff clay, s_u = 100 kPa	Field test	Strain gauge data, back-calculation

Note: (*a*) The critical *s/D* ratio defines the inter-helix spacing where the pile failure transitions from the individual bearing model (IBM) to the cylindrical shear model (CSM); (*b*) All double-helix piles showed IBM, even for piles of *s/D* ratio of 1.5.

Table 3-2. Test pile geometry[a], load test descriptions, and load test results.

Test ID	*s* (mm)	*s/D*	t_s	Q_u[b] (kN)	*T* (kN*m)	K_t (m^{-1})
PA-1[c]	914	3	6 day	-	-	-
PA-2	914	3	15 day	101.5	4.34	23.4
PA-3	914	3	12 day	89.3	3.73	23.9
PA-4	914	3	2 hour	102.7	4.28	24.0
PB-1	457	1.5	16 day	95.4	4.68	20.4
PC-1	1524	5	18 day	93.9	4.11	22.8

Note: (*a*) For all piles: length L = 6.10 m, shaft diameter d = 73 mm, helix diameter D = 305 mm, and helix pitch = 102 mm; (*b*). Q_u defined as load at which pile settlement is 5% of helix diameter, or 15.2 mm; (*c*). Load test without pile rotation constraint on the pile cap.

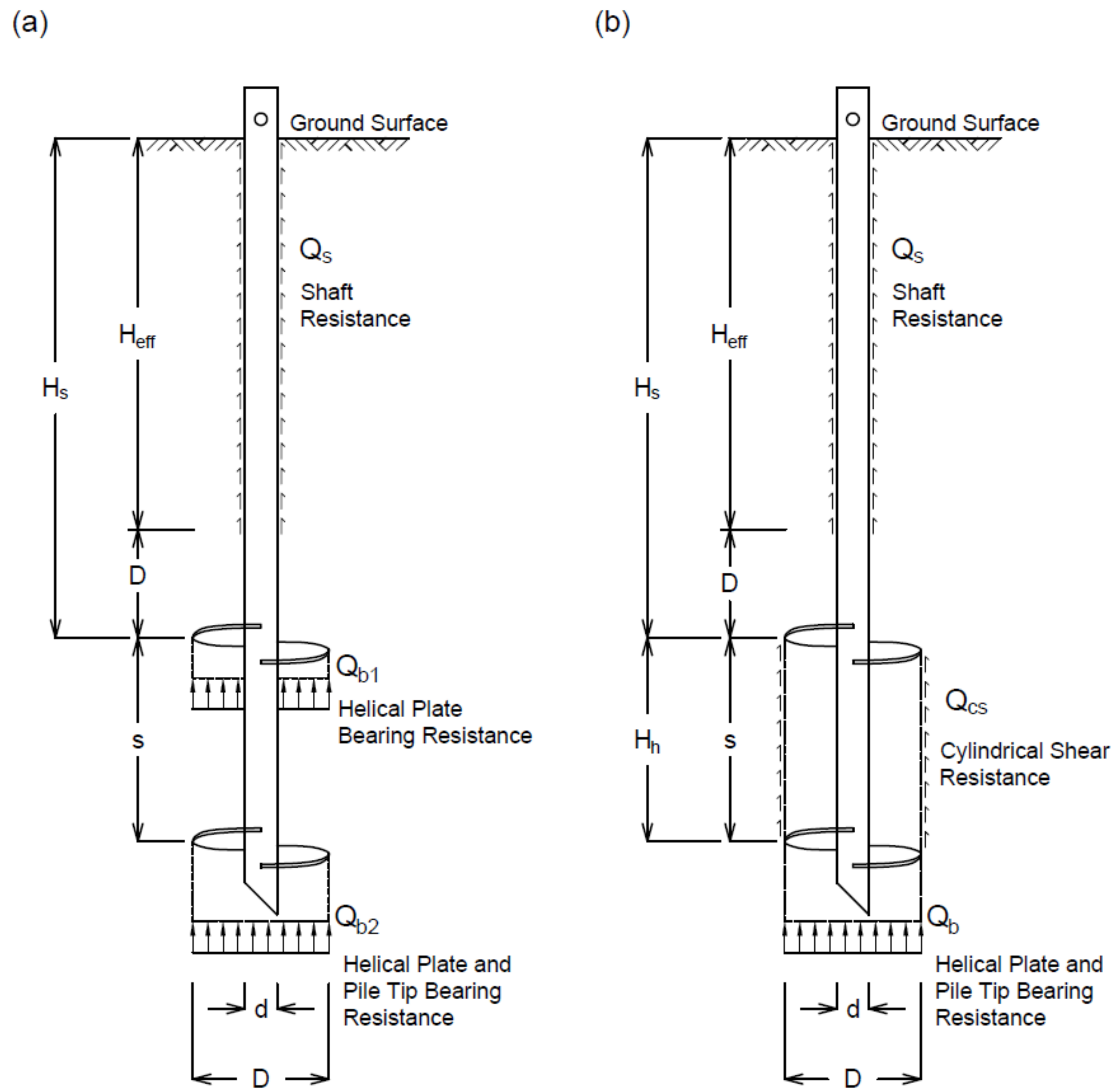

Figure 3-1. Helical pile failure models: (a) individual bearing model (IBM); (b) cylindrical shear model (CSM). After Elkasabgy and El Naggar (2015).

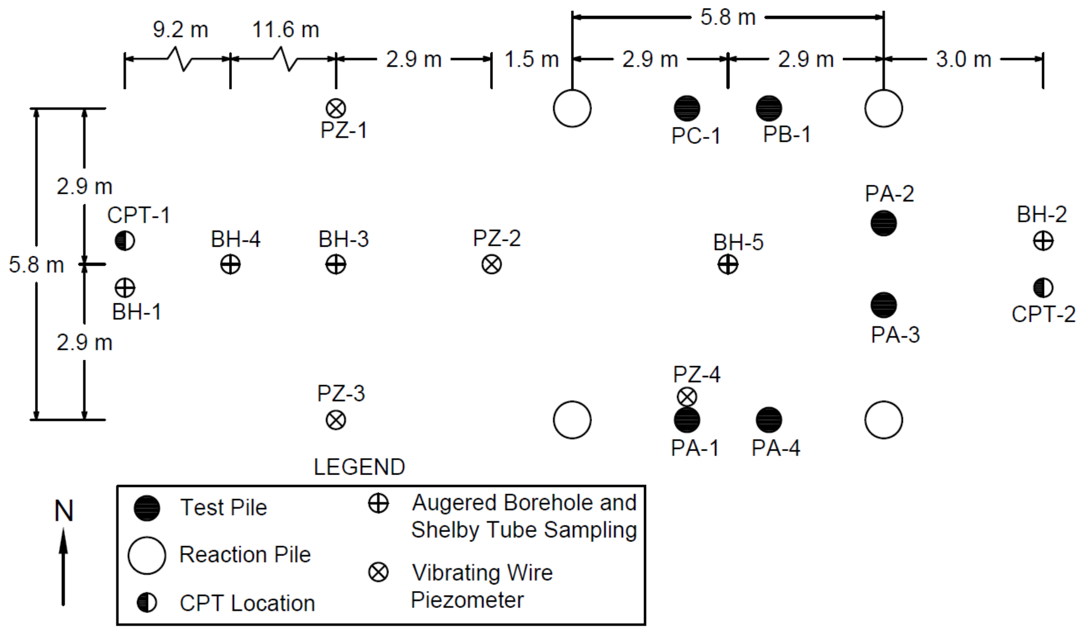

Figure 3-2. Test site layout: test piles, reaction piles, and site investigation activities. Test site location: University of Alberta Farm, Edmonton, Alberta. Geographical coordinate of test site: 53°29’54” N, 113°31’57” W.

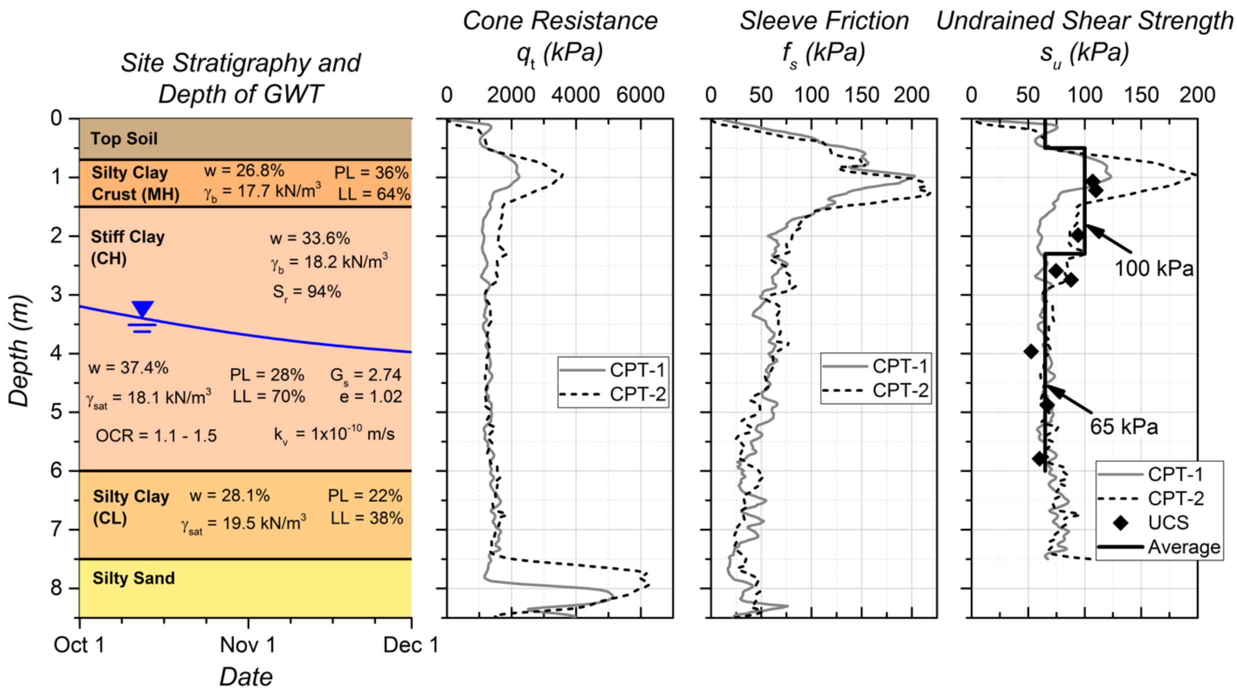

Figure 3-3. Site stratigraphy profile, lab test summary, groundwater table (GWT) depth variation during test period, CPT cone resistance and sleeve friction profiles, and undrained shear strength profile.

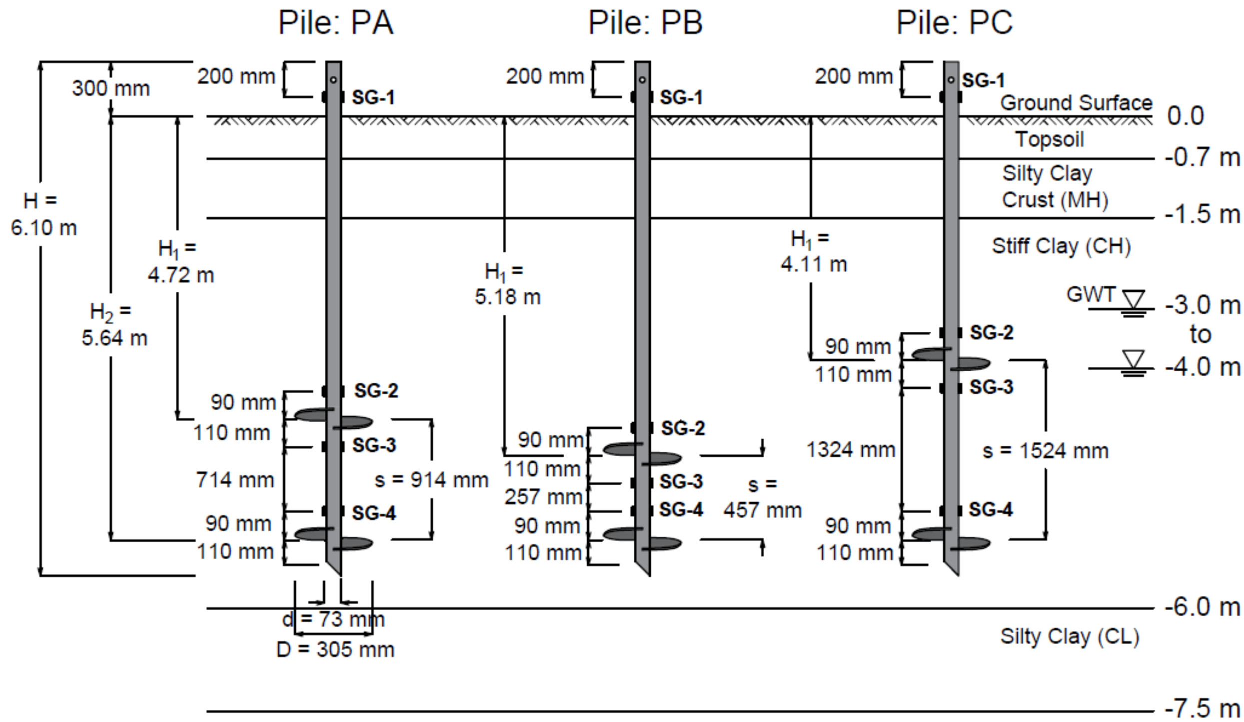

Figure 3-4. Test pile schematic with dimensions and strain gauge station locations with respect to soil layers and groundwater table depth. Note: *H, H*2*, d*, and *D* are equal for all piles. Not drawn to scale.

(a) (b)

Figure 3-5. Strain gauge covers: (a) cylindrical steel cover; (b) covers bolted on a test pile.

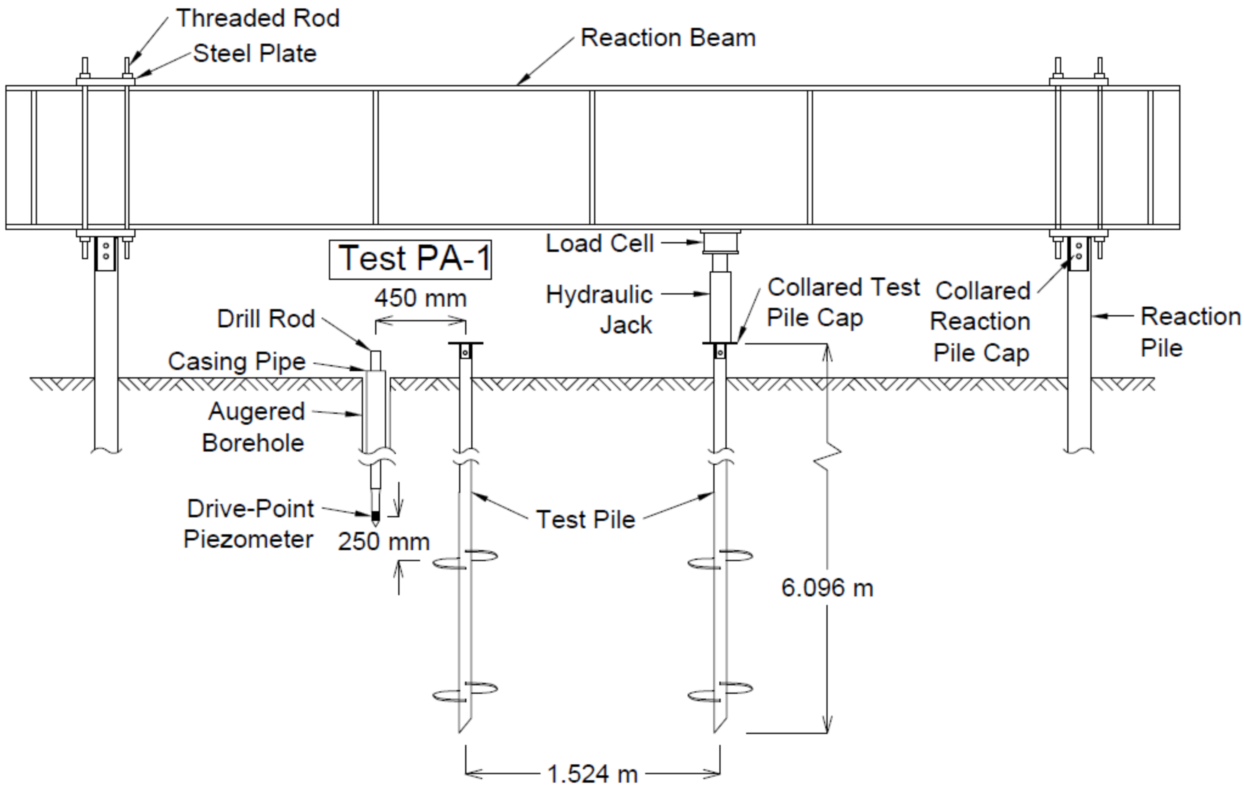

Figure 3-6. Load test setup and piezometer assembly near PA-1. Note: Each reaction beam setup can accommodate two piles, tested sequentially.

Figure 3-7. Load test setup photo.

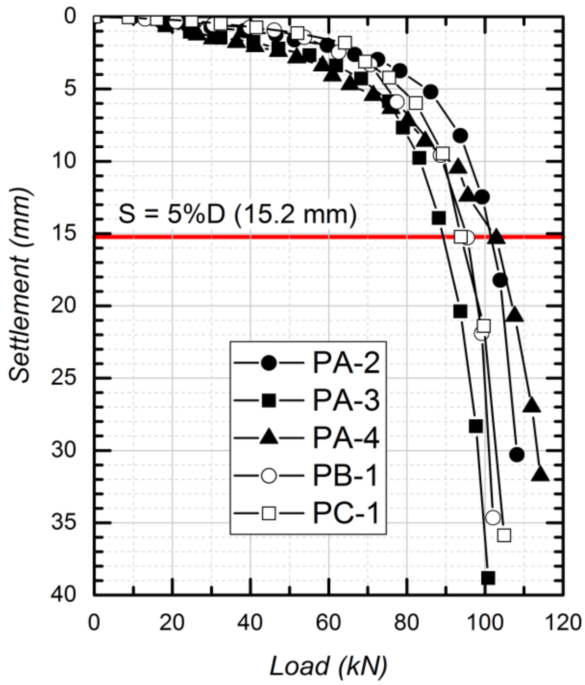

Figure 3-8. Pile-head load versus settlement curves. The ultimate load Q_u is defined at the pile settlement (*S*) at 5% *D*.

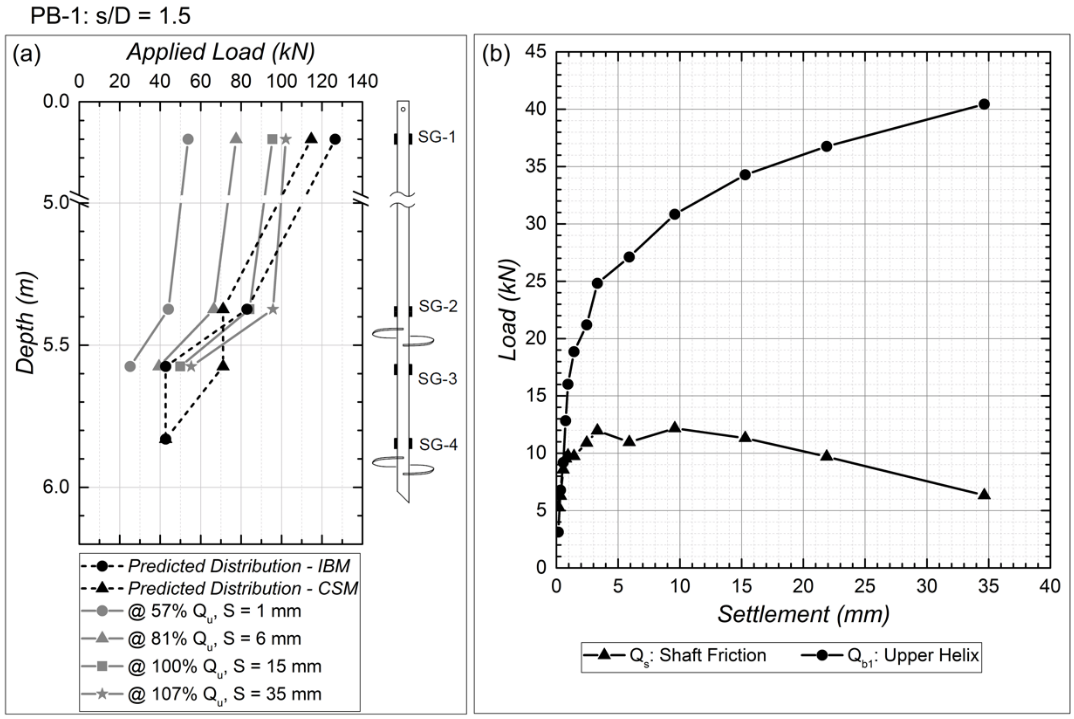

Figure 3-9. PB-1 load distributions: (a) comparison to IBM and CSM predictions; (b) pile component loads. Note: no reliable SG-4 data.

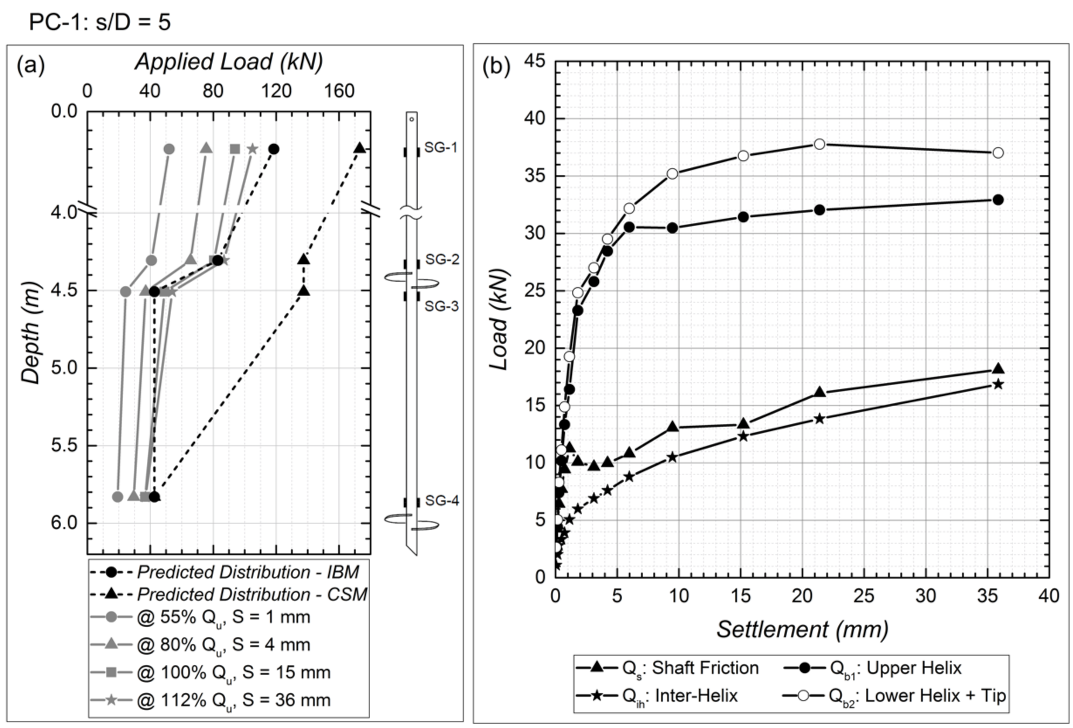

Figure 3-10. PC-1 load distributions: (a) comparison to IBM and CSM predictions; (b) pile component loads.

PA-2: s/D = 3

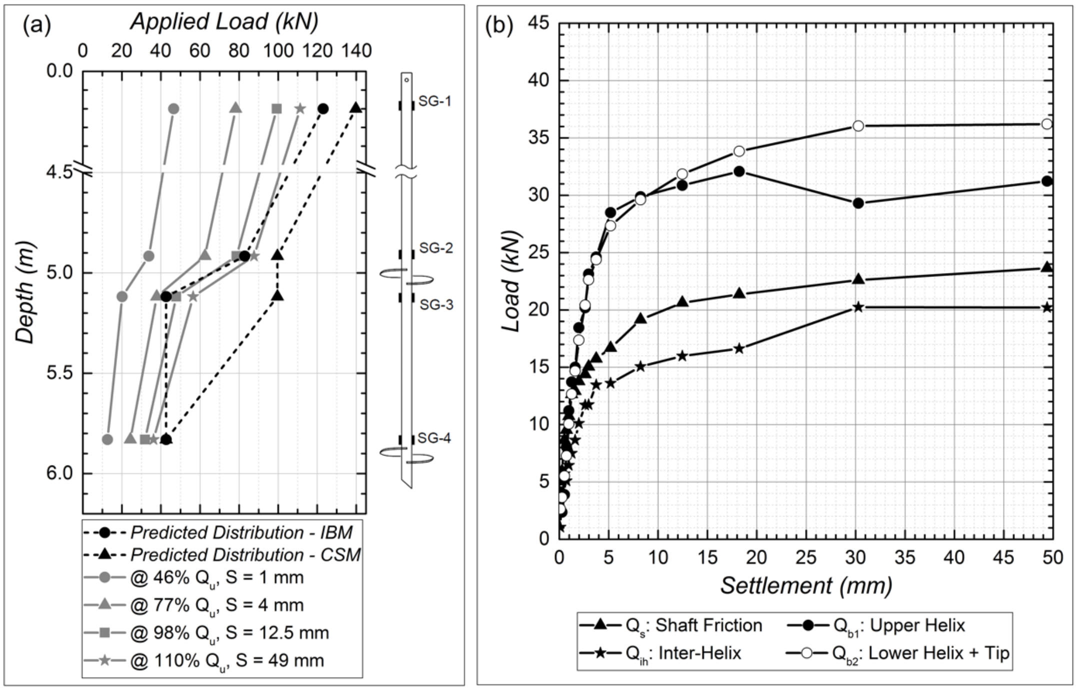

Figure 3-11. PA-2 load distributions: (a) comparison to IBM and CSM predictions; (b) pile component loads.

PA-3: s/D = 3

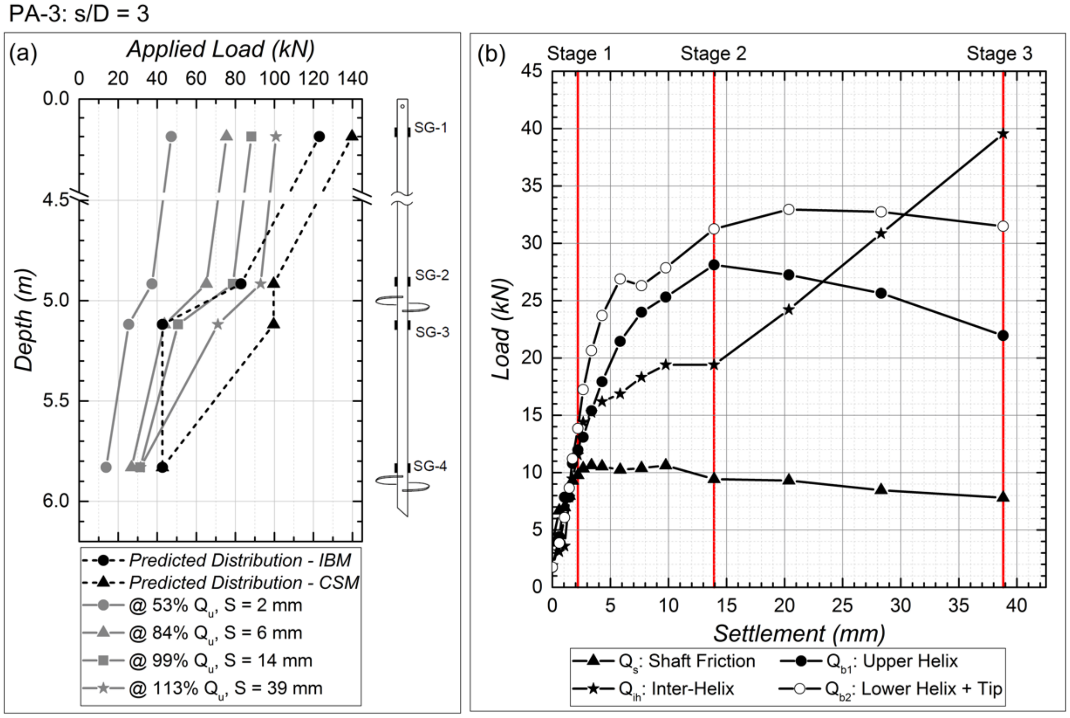

Figure 3-12. PA-3 load distributions: (a) comparison to IBM and CSM predictions; (b) pile component loads. Note: The stages shown in (b) correspond to those in Figure 13.

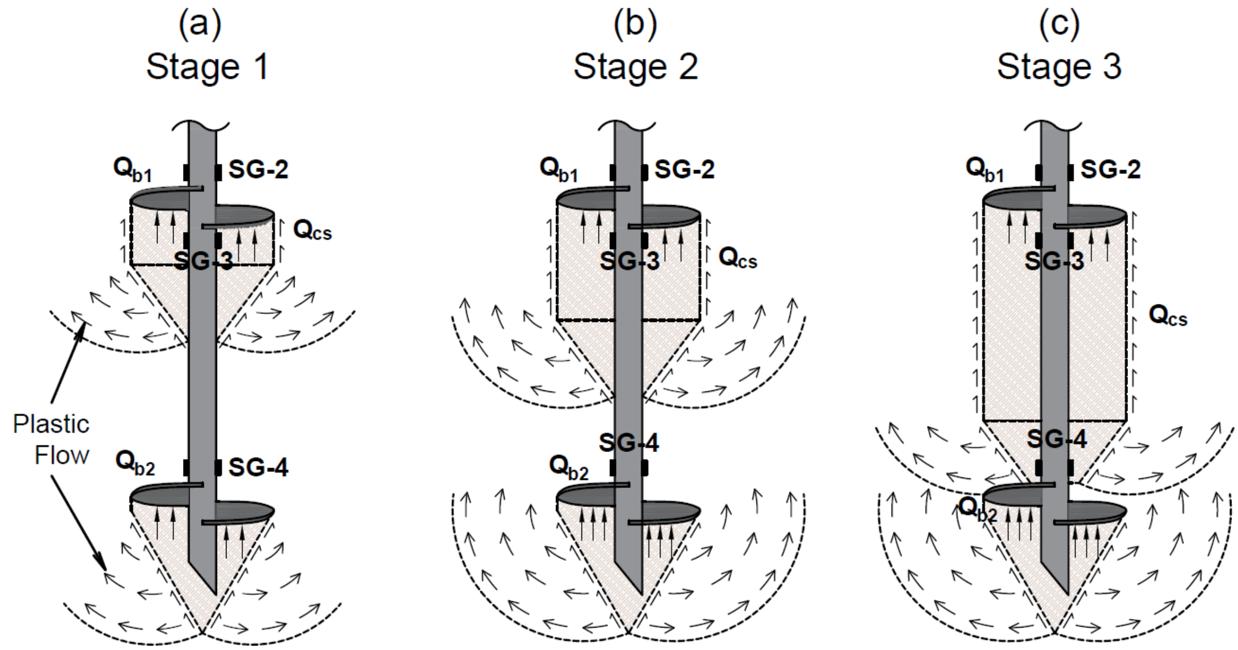

Figure 3-13. Postulated behaviour of PA-3 during the transition between individual bearing and cylindrical shear model. Q_{b1} is the bearing resistance of the upper-helix, Q_{cs} is the cylindrical shear resistance, and Q_{b2} is the bearing resistance of the lower-helix. Note: The stages shown here correspond to those shown in Figure 12b.

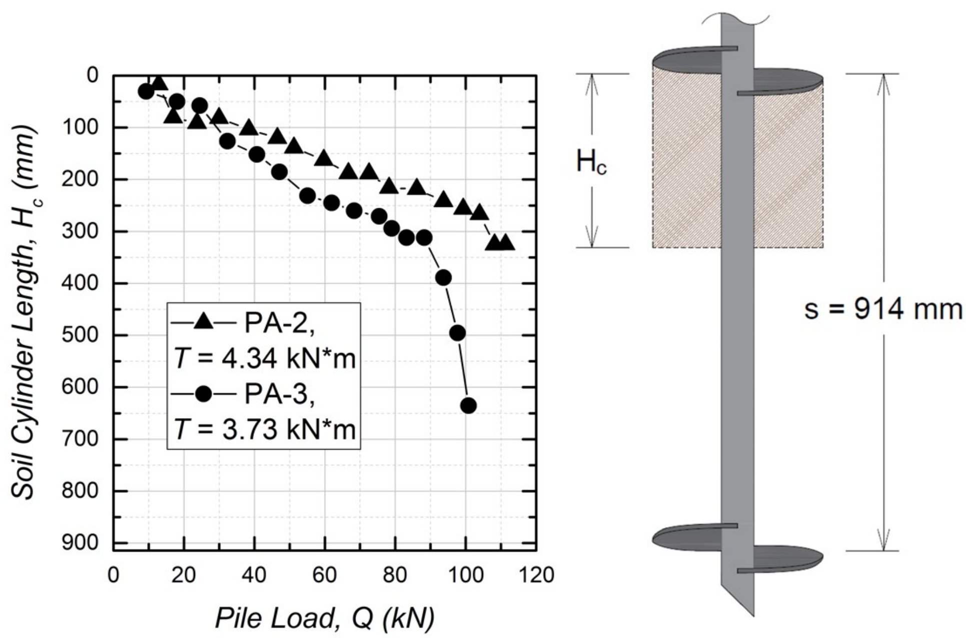

Figure 3-14. Estimated soil cylinder development for PA-2 and PA-3. Note: T is final installation torque.

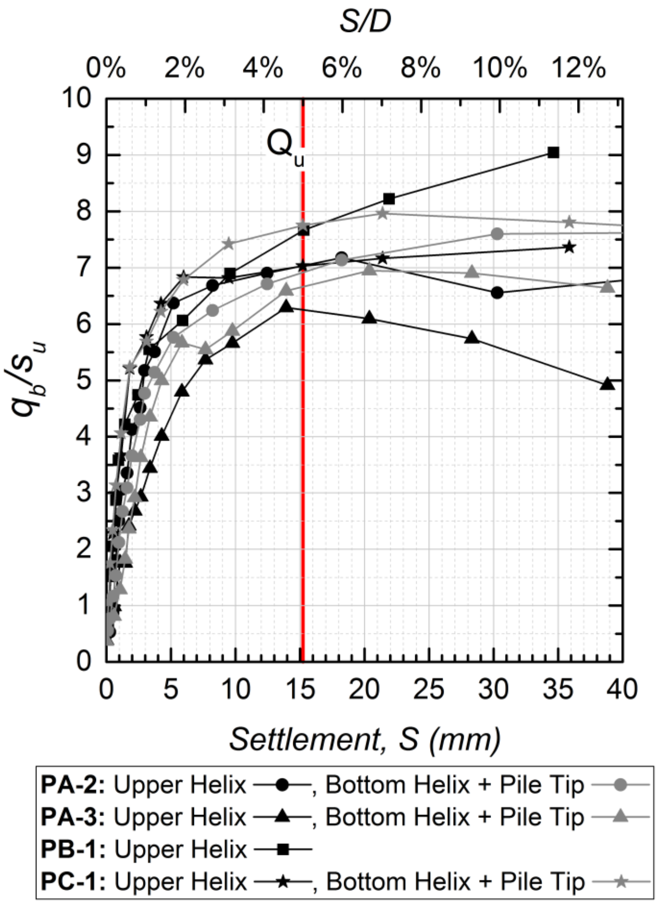

Figure 3-15. q_b/s_u ratio versus pile settlement, where the upper axis shows settlement as a percentage of the helix diameter (D).

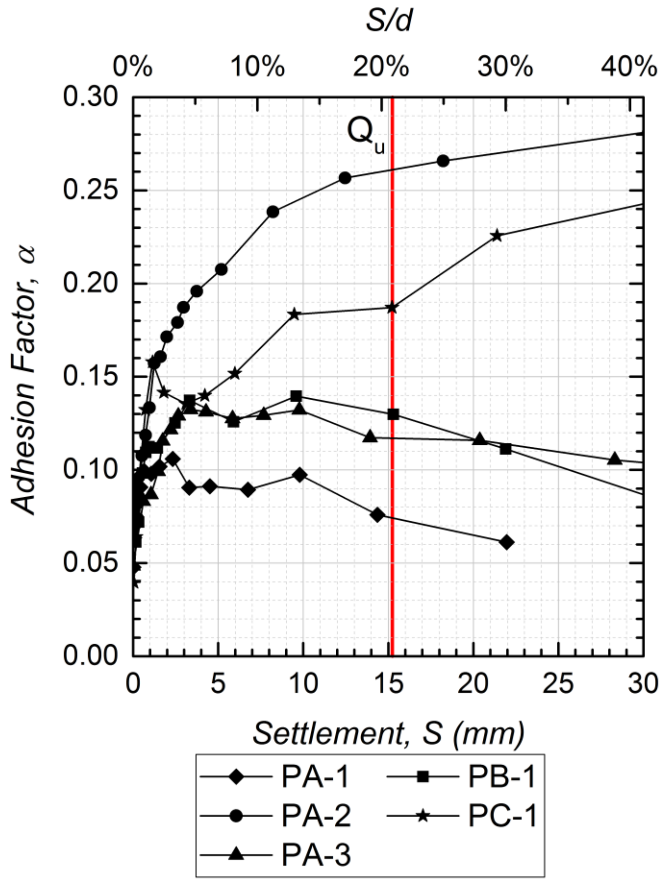

Figure 3-16. Measured shaft adhesion factor (α) versus pile settlement, where the upper axis shows settlement as a percentage of the shaft diameter (d).

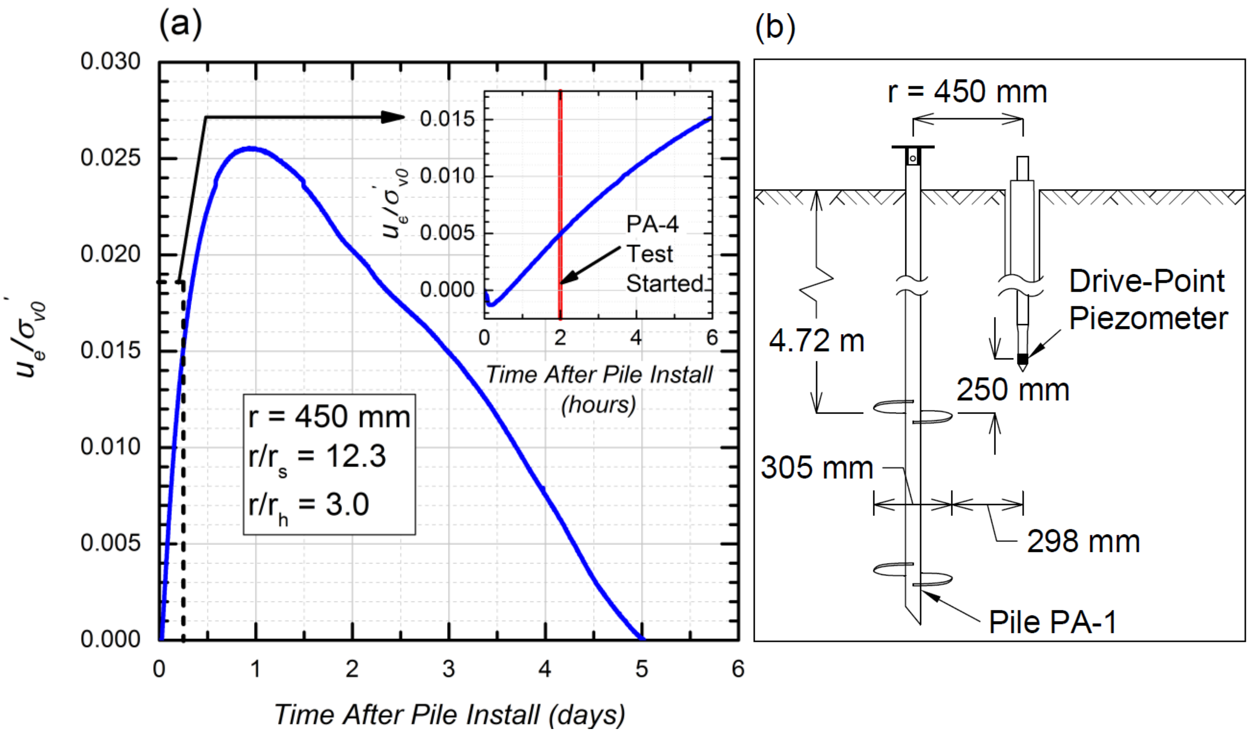

Figure 3-17. (a) Installation-induced excess pore pressure (u_e) generation and dissipation for PA-1; (b) Piezometer location schematic. Note: r is the radial distance from the pile center to the piezometer, r_s is the pile shaft radius, and r_h is the helix radius. PA-4 was tested 2 hours after pile installation.

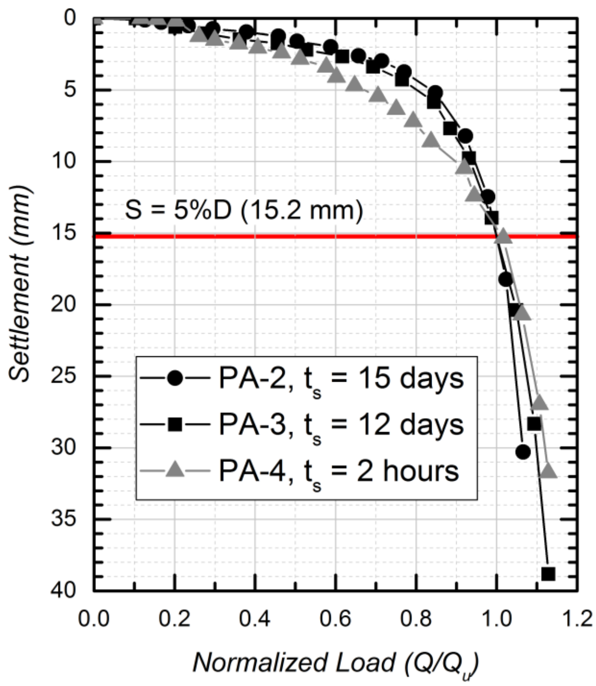

Figure 3-18. Normalized pile load versus settlement. Note: The loads for PA-2 and PA-3 are normalized by their measured ultimate loads and the load for PA-4 is normalized by an estimated ultimate load calculated using the average torque correlation factor (K_t) from PA-2 and PA-3.

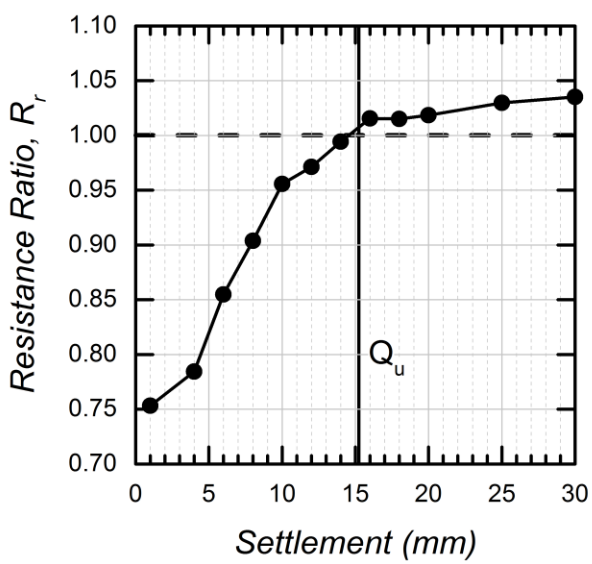

Figure 3-19. Resistance ratio (R_r) of PA-4 versus settlement. R_r is defined in present study as the ratio of Q/Q_u before complete u_e dissipation to Q/Q_u after complete u_e dissipation. R_r of PA-4 is calculated with respect to the average Q/Q_u of PA-2 and PA-3.

4 Axial load testing of helical pile groups in a glaciolacustrine clay[1]

Abstract

The behaviour of helical pile groups has not previously been experimentally investigated through field testing. In the present study, field compressive load tests of 2 × 2 helical pile groups and single piles were conducted in a relatively homogeneous glaciolacustrine clay in Edmonton, Canada. The group pile spacing, inter-helix spacing, and soil setup time were varied. Piezometers were used to measure the excess pore pressure (u_e) response to pile installation. Selected groups contained a strain gauge instrumented pile that was used to estimate the pile load transfer and failure mechanism. Group performance was evaluated by estimating the group efficiencies and settlement ratios. Results show that helical pile group interaction was lower than that of conventional pile groups. The short-term performance of groups was significantly reduced by u_e. The magnitude of u_e at the center of groups increased and the u_e dissipation time decreased as group spacing decreased. Instrumented grouped piles and one single pile, both having an inter-helix spacing ratio of 5, exhibited individual bearing failure. For grouped piles, more load was resisted by the lower-helix than the upper-helix. The measured group capacities and load distributions indicated that individual pile failure occurred, as opposed to block failure.

4.1 Introduction

Helical piles are a deep foundation element composed of one or more steel helical bearing plates welded to a central steel shaft. Piles are screwed into the ground by applying torque and axial force, delivered by a hydraulic drive head. This pile type has various advantages over conventional piles with consistent cross-sections. These advantages include: fast installation,

[1] This chapter has been submitted as Lanyi and Deng (2017b) to the Canadian Geotechnical Journal for possible publication.

light-weight and mobile installation equipment, low noise and vibration during installation, minimal soil disturbance, and pile reusability.

To resist larger loads, helical piles are commonly installed in groups. The application of helical pile groups is especially common for power transmission tower foundations (Adams and Klym 1972). Despite the wide application of helical pile groups, their engineering behaviour, such as their: load-settlement response, installation-induced pore pressure response, effects of soil setup, and failure mode, has not been established in literature. The present study thereby aims to understand the group behaviour by performing field load testing of helical pile groups in a relatively homogeneous glaciolacustrine clay.

4.1.1 General Pile Group Behaviour

Many studies on conventional pile groups (Whitaker 1957; Meyerhof 1960; Poulos 1968) have been directed toward the group effect, which states that closely-spaced piles interact such that their performance is altered. Group performance is reduced when the proximity of neighbouring piles results in the overlap of stress and strain fields. The degree of group interaction increases with decreasing pile spacing, increasing pile length to diameter ratio, and the increasing number of piles in a group (Poulos 1989). Block failure and individual pile failure are two possible failure mechanisms for pile groups. Block failure occurs when the soil between grouped piles fails as a block, while individual failure is characterized by local pile penetration (Whitaker 1957). The likelihood that block failure occurs is higher for groups with closer pile spacing and longer piles, and for groups in cohesive soils (Salgado 2008).

Two metrics are commonly used to evaluate pile group performance: the group efficiency (η_g) and the settlement ratio (R_s). Group efficiency quantifies the reduction in ultimate group capacity; it is defined as (Whitaker 1957):

$$\eta_g = \frac{Q_{ug}/N}{Q_{us}} \qquad \text{[Equation 4-1]}$$

where Q_{ug} is the ultimate group capacity, Q_{us} is the ultimate single pile capacity, and N is the number of piles in the group; the numerator is termed the average group capacity. To evaluate group performance based on settlement, the settlement ratio (R_s) has been adopted for this study, defined as (Poulos and Davis 1980):

$$R_s = \frac{S_g}{S_s} \qquad \text{[Equation 4-2]}$$

where S_g is the settlement of a pile group center and S_s is the settlement of a single pile, evaluated when the average group load equals the single pile load.

4.1.2 Helical Pile Group Behaviour and Past Research

The group behaviour of helical piles may differ from that of conventional piles due to the unique geometry of this pile type. For helical piles, the helix diameter is always larger than the shaft diameter, while conventional piles often have cylindrical shafts with an equal-diameter toe and shaft. Group pile spacing is often described by the ratio of the pile center-to-center spacing (s_g) to pile toe diameter (D) for conventional pile groups, or to the helix diameter (D) for helical pile groups. At equal s_g/D ratios, the shaft spacing within helical pile groups will be greater than in conventional pile groups. Figure 4-1 shows a schematic of the stress fields around a conventional pile group and a helical pile group. The dotted lines represent shear stress isochrones. These stress distribution are for visualization purposes only, as they have not been verified through field testing or numerical modelling. In Figure 4-1, both groups have equal s_g/D ratios; however, the shaft diameter (D) of the conventional pile group is greater than that of the helical pile group (d), thus, resulting in less shaft interaction in the helical pile group.

Trofimenkov and Mariupolskii (1965) performed field pullout tests on groups consisting of three helical piles in a row and found that there was no group resistance reduction when $s_g/D \geq 1.5$. Shaheen and Demars (1995) performed laboratory pullout tests of model anchor groups in sand. They determined that in dense sand helical pile group capacity reduced exponentially as group spacing decreased; in loose sand, however, group performance was independent of group spacing. Elsherbiny (2011) evaluated helical pile group performance using the finite element method (FEM). It was found that η_g of a 2×2 helical pile group was greater than that of conventional pile groups because soil displacement around the helices was localized. Perko (2009) suggested that the soil in the inter-helix region between grouped piles may fail as a block, and that Q_{ug} may be estimated by summing the bearing resistance of the base of the block and the soil shear resistance along sides of the block:

$$Q_{ug} = q_{b,ult} m_1 m_2 + 2 s_u (n-1)(m_1 + m_2) s \quad \text{[Equation 4-3]}$$

where $q_{b,ult}$ is the ultimate state unit base resistance of the block, m_1 and m_2 are the width and breadth of the group bounded by the helices, n is the number of helices per pile, s is the inter-helix spacing, and s_u is the undrained shear strength of soil.

4.1.3 Installation Disturbance and Soil Setup in Cohesive Soils

The screwing action during helical pile installation causes soil to displace outward from the pile shaft and to be sheared by the helical plates cutting through the soil. This installation disturbance causes a change in the soil stress state near the pile and may alter the shear strength of fine-grained soils (Weech 2002). The change in soil stress may be the result of two factors: the increase in total stress, caused by the penetration of the pile shaft forcing soil radially outward from the shaft (Poulos and Davis 1980); and the change in effective stress due to the volumetric response of fine-grained soils to shear strain (Randolph 2003). The increase in total stress will result in positive excess pore pressure (u_e), but a soil's response to shear strain depends on the overconsolidation ratio (OCR) (Weech 2002). Since s_u is dependent on the magnitude of u_e, s_u will vary as pore pressure equilibrates. The dissipation of u_e, resulting in an increase in pile capacity with time, is known as soil setup. The rate of soil setup is directly related to the rate of consolidation near the pile (Soderberg 1962). Weech (2002) conducted a field investigation on the soil disturbance caused by a single helical pile installation in a highly-sensitive marine clay; u_e at the pile shaft wall and at several locations away from the pile was measured and pile capacities at several setup times were determined.

Thus far, soil setup around a helical pile group has not been studied. Pile grouping may alter the u_e regime in the vicinity of a pile group. Soderberg (1962) noted that as group pile spacing decreases, u_e near the piles increases due to the compounding influence of closely spaced piles, and the dissipation duration decreases due to a shortened drainage path. For helical pile groups, however, the interaction of u_e and group performance has not yet been investigated.

4.1.4 Torque – Capacity Relationship

Research has shown that the installation torque measured during pile installation can be used as an indicator of the shear strength of soil traversed by the pile and the pile's capacity. Hoyt and Clemence (1989) developed an empirical equation relating the final installation torque (T) to ultimate capacity (Q_{us}) of a single helical pile:

$$Q_{us} = K_t \cdot T \qquad \text{[Equation 4-4]}$$

where K_t is the capacity-torque ratio.

4.1.5 Helical Pile Load Distribution - Individual Bearing Model

An axially-loaded helical pile's failure surface can be described by the individual bearing model (IBM) or the cylindrical shear model (CSM). The IBM predicts that bearing failure occurs at each helix and that there is negligible interaction between adjacent helices (Elkasabgy and El Naggar 2015). Past studies have found that the IBM dominates pile behaviour when the *s/D* ratio is greater than 1.5 (Rao et al. 1993; Rao and Prasad 1993) or 3 (Zhang 1999; Tappenden 2007). The ultimate capacity (Q_{us}) predicted by the IBM in an undrained condition is estimated as:

$$Q_{us} = Q_{bearing} + Q_{shaft} = N_t s_u A_b n + \alpha s_u \left(\pi d H_{eff} \right) \qquad \text{[Equation 4-5]}$$

where $Q_{bearing}$ is the sum of bearing resistance of all helical plates, Q_{shaft} is the shaft resistance, N_t is a bearing capacity coefficient, A_b is the helical plate bearing area, α is the adhesion coefficient, d is the shaft diameter, and H_{eff} is the effective shaft length. The CFEM (2006) suggests an N_t value of 9 when the pile toe diameter is less than 0.5 m and α between 0.5 and 1.0. Perko (2009) suggests a lower α for helical piles due to poor soil-shaft contact caused by wobbling during pile installation. H_{eff} is the length of shaft that contributes to Q_{shaft}; it can be estimated as the shaft length above the lower-helix (H_s) minus 1D per helix, to account for a void forming above each helix (Elkasabgy and El Naggar 2015).

4.2 Objectives and Scope

The present study examines the behaviour of helical pile groups under axial compressive loading in a relatively homogeneous glaciolacustrine clay. Seven pile groups and four single piles were tested at the University of Alberta farm site in Edmonton, Canada. The objectives of this study are to: (i) evaluate the effects of the s_g/D ratio on group performance; (ii) determine the effects of the s_g/D ratio on the installation-induced u_e near the piles; (iii) evaluate the effects of u_e on group performance; and (iv) determine the load transfer and the failure mechanism of a pile group.

Pile groups consisting of four piles in a square pattern, and single piles for comparison, were tested under axial compressive loads. All test piles had two helices. The group pile spacing and inter-helix spacing were varied among tests. Piezometers were installed at the center of selected pile groups and near a single pile to measure the u_e response to pile installation. The soil setup time (i.e. the time between pile installation and loading) was varied for two group configurations. One set of tests was performed 5 hr after pile installation, while another set was performed 7 to 9 days after installation when u_e had dissipated. Selected test piles were instrumented with strain gauges for estimating the load transfer and failure mechanism along these piles.

4.3 Test Site and Investigation

The testing program took place at a cohesive soil site at the University of Alberta farm in Edmonton, Canada. The subsoils in this area consist of Glacial Lake Edmonton sediments overlying till, representing a typical soil profile of the Edmonton area. The glaciolacustrine sediments were deposited near the end of the Wisconsin glacial period, as a result of the formation of Glacial Lake Edmonton, approximately 12,000 years ago (Godfrey 1993).

A comprehensive site investigation was conducted prior to and during the testing program, which included cone penetration testing (CPT), Shelby tube sampling, lab soil testing, and piezometer installations. Figure 4-2 shows the locations of the site investigation activities with respect to the test pile locations.

The soil stratigraphy profile was determined using CPT data and laboratory characterization testing of sampled soils. Previous knowledge of the site geology (Bayrock and Hughes 1962) and a review of past investigations near the site (Zhang 1999; Tappenden 2007) also assisted in interpreting the soil layers. As shown in Figure 4-3, beneath 0.7 m of topsoil, there is a 0.8-m-thick clayey silt crust underlain by a 4.5-m-thick stiff glaciolacustrine clay deposit. At a depth of 6.0 m there exists a 1.5-m-thick layer of interbedded silty clay with sand seems. From 7.5 to 9.5 m below the ground surface, the soil consists of a silty sand deposit with interbedded silty clay;

this layer is underlain by till at a depth of 9.5 m. Throughout the testing program, the groundwater table (GWT) depth was measured directly with a piezometer. It was found that the GWT varied from 3.0 m deep in September to 4.0 m deep in December 2016.

Laboratory soil classification testing and strength testing was conducted on soil from boreholes BH-1 to BH-4, from depths between 0.75 and 6.55 m. Soil classification testing included: Atterberg limits, moisture content (w), bulk unit weight (γ_b), and specific gravity of solids (G_s). To determine s_u, unconfined compressive strength (UCS) testing was performed. Consolidation testing was performed on two samples from BH-5, at depths of 4.72 and 5.33 m. The deposit of most interest was the saturated glaciolacustrine clay layer because the helical plates of the test piles would be situated below the GWT in this layer. The properties of the saturated glaciolacustrine soil are as follows: γ_{sat} of 18.1 kN/m^3, liquid limit (LL) of 70%, plastic limit (PL) of 28%, w of 37.4%, OCR between 1.1 and 1.5, and a vertical hydraulic conductivity of approximately 1×10^{-10} m/s. The Atterberg limits indicated that the glaciolacustrine clay had a USCS classification 'CH', or a fat clay. Figure 4-3 shows a summary of the lab test results.

Equation 4-6 (Robertson and Cabal 2015) was used to estimate the in-situ s_u of the cohesive soil at this site:

$$s_u = \frac{q_t - \sigma_v}{N_{kt}} \quad \text{[Equation 4-6]}$$

where q_t is the corrected cone tip resistance, σ_v is the overburden stress, and N_{kt} is an empirical factor (typically ranging from 10 to 18). Based on findings from a previous investigation near this site (Tappenden 2007), an N_{kt} value of 18 was used. A good agreement between the in-situ s_u and laboratory-measured s_u was observed (Figure 4-3). UCS tests of the saturated stiff clay (CH) layer found s_u to vary between 55 and 67 kPa, whereas s_u estimated from Equation 4-6 varied between 57 and 77 kPa. Comparing f_s to s_u showed that the stiff clay (CH) had a sensitivity (S_t) less than 2 throughout this layer.

4.4 Load Test Program

The field test program consisted of axial compression loading of seven 2 × 2 helical pile groups and four single piles. Testing was conducted from September to December of 2016.

4.4.1 Test Pile and Load Test Description

Double-helix test piles were manufactured and installed for this project. All test piles had a length (L) of 6.10 m, a closed-ended shaft of 73-mm-diameter (d), two 305-mm-diamter helices (D), a helix pitch of 102 mm, and an inter-helix spacing (s) of 914 mm or 1524 mm. Figure 4-4 shows a schematic of the test pile geometries and the location of the helices with respect to the soil stratigraphy.

Table 4-1 shows a summary of all pile tests. Groups with an s/D ratio of 3 (PG-A1 to PG-C2 in Table 4-1) had varied group-pile-spacing ratios (s_g/D = 2, 3, and 5). For groups with an s_g/D ratio of 2 and 3, the soil setup time (t_s) was also varied. Tests PG-B2 and PG-C2 occurred 5 hr after pile installation, while tests PG-B1 and PG-C1 occurred 8 to 9 days after pile installation. The single pile tests P-2 and P-3 (s/D = 3) were performed so the load settlement response of pile groups could be compared to that of single piles. The performance of PG-D1 and PG-D2 (s/D = 5) could not be evaluated since differential group pile settlement during testing prevented these groups from reaching their ultimate capacities. However, the load transfer data from the instrumented piles within these groups was useful for the load transfer analysis. The single pile P-4 (s/D = 5) was also instrumented in order to differentiate the behaviour between groups and single piles.

4.4.2 Instrumentation

Drive-point vibrating wire piezometers were used to measure the pile installation-induced u_e generation and dissipation at the center of groups PG-B1 and PG-C1 and near the single pile P-1. The baseline piezometer readings were also used to measure the depth of the GWT throughout the testing program. The piezometer consisted of a 25-mm-diameter hollow steel shaft with a coned tip. Figure 4-5 shows a schematic of the piezometer assembly and installation method. The piezometer was screwed onto a drill rod to allow the assembly to reach the desired depth. Before installing the piezometers, a 150-mm-diameter borehole was drilled with an auger to a depth of 3.7 m, and cased with a steel pipe to prevent soil sloughing. The piezometer was then placed into the steel pipe and pushed the remaining 1.0 to 1.5 m to the target depth. The borehole was required because pushing the piezometer from the surface may have over-ranged the vibrating wire diaphragm. For the group tests, the depth of the piezometer tip was 5.2 m below the ground surface, or 500 mm below the upper-helix; for the single pile P-1, the depth of the piezometer tip was 4.5 m below ground surface, or 250 mm above the upper-helix.

One of the four piles in PG-D1 and PG-D2, and the single pile P-4, were instrumented with electrical resistance strain gauges at four stations along the pile shafts. Figure 4-4 shows a schematic of the strain gauge stations (SG-1 to SG-4) on a test pile. With this gauge configuration, the load resisted by each pile component (upper-shaft, upper-helix, inter-helix, lower-helix) could be resolved. A Wheatstone full-bridge circuit was used at each station. To prevent damage to the gauges during pile installation, steel covers were used at the gauge locations. The covers consisted of two hollow half-cylinder steel pieces that fit together around the shaft to form a continuous steel barrier. The covers were 100 mm long and 15 mm thick. To fasten the covers to the shaft, a threaded rod ran through the cover and the shaft through clear drill holes and was bolted at both ends. Because of the bolting method, the covers did not change the shaft stiffness at the gauge stations. Before installing the covers, an epoxy and a polymer-based water-resistant coating were applied to the gauges surface.

A 980-kN-capacity hydraulic jack was used to apply a load to the test piles. A load cell was used to measure the applied load. Axial pile displacements were measured using linear potentiometers (LPs). For pile group tests, one LP was installed at each of the group's four corners; for single piles, one LP was fastened to either side of the loading plate. The LPs and the load cell were calibrated prior to the testing program. A data logger, with a 5-sec sampling interval, was used to record the measurements. Installation torque was measured with an electronic torque monitor and recorded manually every 0.3 m of pile penetration.

4.4.3 Load Test Configuration

A typical configuration is shown in Figure 4-5. The reaction beam was a 7-m-long W840×299 I-beam and the reaction piles were spaced 5.8 m apart (Figure 4-2). The reaction piles for pile group tests were 7.9 m long, with a shaft diameter of 140 mm and four helices of 457-mm diameter; the reaction piles for individual pile tests were 6.1 m long, with a shaft diameter of 140 mm and three helices of 457-mm diameter. During pile testing, no axial displacement of the reaction piles was observed. Pile groups were centered between adjacent reaction piles; single test piles were spaced 1.52 m apart, with at most two test piles centered between two reaction piles (Figure 4-2). The minimum center-to-center spacing between test and reaction piles was five helix diameters of the larger pile.

A pile cap was required for pile group tests. The cap consisted of three I-beams configured in an 'H' pattern, as shown in Figure 4-6. The two lower-cap I-beams (W250×49) running parallel to the reaction beam had slotted bottom flanges so they could be bolted to the test piles below.

The upper-cap I-beam (W310×97) was seated at the center of the two lower beams, aligned perpendicular to the reaction beam.

Due to the pitch of the helices, a single helical pile may rotate under axial loading. In practice, this rotation is unlikely because the pile cap is fixed to the superstructure. To prevent pile rotation during single pile tests, a collared loading plate with a hooked end was bolted to each test pile. A chain was connected to the hook on the loading plate and wrapped around the nearest reaction pile. The chain was then tightened to provide a moment to resist pile rotation.

4.4.4 Load Test Procedure

All pile testing followed the ASTM (2007) "quick test" axial compression load test procedure (D1143/D1143M – 07). The applied load was increased in increments of approximately 5% of the estimated design load. During each increment, the load was held for 5 min to allow the rate of pile settlement under the sustained load to approach zero. Individual piles were loaded until additional settlement resulted in no further increase in pile resistance (known as plunging failure). For pile group tests, it was not always possible to reach plunging failure. Differential settlement between piles in the groups caused tilting of the hydraulic jack at high loads. For groups with excessive differential settlement, testing progressed until it was deemed no longer safe to increase the load. After reaching the maximum load, unloading occurred in five approximately equal decrements.

4.5 Results and Discussion

4.5.1 Differential Group Pile Settlement

An unintended consequence of the group pile cap design was that it allowed for differential settlement between the individual piles within a group. To mitigate differential settlement, all grouped piles were installed to the same elevation and the load was applied as close as possible to the group's center. However, differential settlement still occurred to some extent. The differential settlement between two piles in a rigidly connected set (i.e. under the same lower-cap I-beam) was generally low (< 5 mm) at the ultimate state, whereas the differential settlement between two sets of piles was in some cases as much as 20 mm.

The effects of installation disturbance on differential settlement were investigated by comparing the installation order of grouped piles to the final installation torques (T) of those piles. There was no clear correlation between the installation order and T; further, the pile installation-induced u_e data (discussed later) indicate negligible disturbance at a distance of $2D$ (i.e. the minimum s_g of all groups) away from a pile.

As eccentric loading and installation disturbance were ruled out, it was theorized that the differential settlement was caused by varied soil strength in the vicinity of grouped piles. As an example, Figure 4-7 shows the pile installation torque profiles and the group load versus individual pile settlement curves of PG-B2. For the locations of the individual piles within PG-B2, refer to Figure 4-2. It is shown in Figure 4-7 that a higher T resulted in a lower individual pile settlement. For example, the SE pile, which had a higher T than other piles, had a stiffer load – settlement response and less settlement than other piles. The respective T of each pile in a rigidly connected set appeared to have influenced the settlement of the other pile in the set. This is shown by the SW and SE piles, in a set, having a similar load – settlement curve even though T of the SW pile was much less than T of the SE pile. In the other set, the NW and NE piles had a similar T and a similar load – settlement curve.

To visualize the torque-settlement relationship, T and S of the piles in rigidly connected sets were averaged. Figure 4-8 shows the average torque (T_{avg}) versus the average settlement (S_{avg}) for pile sets of several of the group tests, where S_{avg} was measured at Q_{ug}. Figure 4-8 shows that groups with significantly varying T_{avg} also had significant differential settlement between pile sets at Q_{ug}; the set with a higher T_{avg} had a lower S_{avg}.

It was thus concluded that the primary cause of group differential settlement was local soil strength heterogeneity. It was important to understand the mechanism of the differential settlement in order to have confidence in, and to aid in interpreting, the group load test results. Also, differential settlement had to be considered when selecting the group failure criterion.

4.5.2 Selection of Failure Criterion

For single piles, failure is generally defined by the limit load, i.e. the load causing plunging; however, differential settlement made it difficult to reach the limit load for all group tests. Therefore, a settlement-based failure criterion was adopted. Elkasabgy and El Naggar (2015) recommended that the ultimate load (Q_u) should fall within the nonlinear region of the load-settlement curve, where creep settlement is low. Based on this recommendation and from inspection of the load-settlement curves, Q_u adopted for this study was defined as the load causing pile settlement of 5% of the helix diameter, or 15.2 mm. This 5%D criterion was also adopted for the helical pile studies by Elsherbiny and El Naggar (2013) and Lanyi and Deng (2017a). At 5%D, creep settlement was negligible and differential settlement between grouped piles was smaller than that at higher loads.

Figure 4-9 shows the load-settlement curves for the pile groups and single piles P-2 and P-3. For pile groups, the applied group load was plotted against the settlement of the pile group center, determined using the LP readings at the group's corners. Following the 5%D criterion, Q_u of all applicable tests are summarized in Table 4-1. For PG-D1 and PG-D2, Q_{ug} could not be obtained due to excessive differential settlement; therefore, the performance of these groups was not evaluated.

4.5.3 Metrics of Group Performance

To quantify the group effect and to evaluate pile group performance, the load-settlement curves of the groups were compared to that of P-2 and P-3. A capacity-based evaluation was made by calculating η_g (Equation 4-1). A settlement-based evaluation was made by calculating R_s (Equation 4-2) at selected pile group factors of safety (FS), where FS was defined as the ratio of the measured Q_{ug} to the pile group load (Q_g). The pile group and single pile load-settlement behaviour could not be directly compared without considering T, since T varied among the piles. To mitigate the effect of T on η_g and R_s, the single pile load (Q_s) and pile group load (Q_g) were normalized. The normalized single pile load ($\overline{Q}_s$) was calculated using Equation 4-7:

$$\overline{Q}_s = \frac{Q_s}{Q_{us}} \qquad \text{[Equation 4-7]}$$

where Q_{us} is the measured ultimate capacity of single piles. The value of Q_g was normalized by the sum of the estimated ultimate capacities of the single piles in each group, which were calculated using the torque-capacity relationship (Equation 4-4), as shown in Equation 4-8:

$$\overline{Q}_g = \frac{Q_g}{\sum_{i=1}^{N}\left(K_t \cdot T_i\right)} \qquad \text{[Equation 4-8]}$$

The K_t factor used in Equation 4-8 was an average (23.65 m^{-1}) determined from P-2 and P-3 (Table 4-1).

The normalized loads $\overline{Q}_s$ and $\overline{Q}_g$ were plotted against settlement (Figure 4-10). After normalization, the P-2 and P-3 curves became very consistent. The value of η_g equals the ratio of $\overline{Q}_g$ to the average $\overline{Q}_s$ of P-2 and P-3 at a settlement of 5%D (15.2 mm). The value of R_s equals the ratio of S_g to the average S_s of P-2 and P-3 at equal normalized loads ($\overline{Q}_g = \overline{Q}_s$), at a given pile group FS.

4.5.4 Effects of the s_g/D ratio on Group Performance

The effects of group pile spacing on group performance were investigated by performing group load tests with varied s_g/D ratios. Pile group tests PG-A1, PG-B1, and PG-C1 with s_g/D ratios of 5, 3, and 2, respectively, were carried out; these groups had s/D ratios of 3. All these tests had a $t_s \geq 7$ days to allow for complete u_e dissipation (discussed later). To compare the performance of helical groups to conventional pile groups, η_g was estimated using the Converse-Labarre equation (Bolin 1941), an empirical formula commonly used to estimate η_g of conventional piles (Hanna et al. 2004):

$$\eta_g = 1 - \frac{\theta\left[\left(N_1 - 1\right)N_2 + \left(N_2 - 1\right)N_1\right]}{90 N_1 N_2} \qquad \text{[Equation 4-9]}$$

where $\theta = \arctan(D/s_g)$, N_1 is the number of rows in a group, and N_2 is the number of columns.

Figure 4-11 shows η_g of the three tests along with η_g estimated using the Converse-Labarre equation and η_g estimated by Elsherbiny (2011). The results from this study could be compared to the FEM results from Elsherbiny (2011) because the soil properties, pile geometries, and group configurations from both studies were similar (Elsherbiny: s_u = 75 kPa, L = 6.2 m, d = 273 mm, D = 610 mm, n = 2, s/D = 3, 2×2 group). It was found that η_g decreased with a deceasing s_g/D ratio. The values of η_g were 96.8%, 95.5%, and 90.7% at s_g/D ratios of 5, 3, and 2, respectively. The magnitude and trend of the measured η_g matched closely with Elsherbiny (2011) predicted values, although the measured values were 1 to 2 percentage points higher. The measured η_g values were consistently much higher than the Converse-Labarre equation predicted values, indicating that the interaction of helical piles groups was lower than that predicted for conventional pile groups with equal s_g/D ratios.

Figure 4-12 shows the measured R_s for PG-A1, PG-B1, and PG-C1 plotted at pile group FS of 1, 1.5, and 2. The values of R_s were only estimated up to the group FS of 2 because the values of S_g and S_s at loads corresponding to FS > 2 were so small (< 1 mm) that the accuracy of R_s was low. At all FS values, R_s was found to increase with a decreasing s_g/D ratio. At FS of 1 (i.e. at Q_{ug}), R_s was 1.88, 1.38, and 1.26 at s_g/D ratios of 2, 3, and 5, respectively. At higher FS (lower load), R_s was reduced, indicating lower group interaction. At FS of 2, all groups had a value of R_s below 1.0, indicating that the groups had a stiffer response than the single piles under low loads.

The findings from the present study show that group interaction increased (indicated by a higher R_s) as the load increased. In contrast, Elsherbiny (2011) found that R_s decreased as the load increased, as the FEM estimated displacement fields extended further at lower loads than at higher loads.

4.5.5 Installation-Induced Pore Pressure

Pile installation-induced u_e was measured for P-1, PG-B1, and PG-C1. For P-1, the piezometer was installed at a radial distance (r) of 450 mm from the shaft center, corresponding to a r/r_{shaft} ratio of 12.3, where r_{shaft} is the pile shaft radius. For PG-B1 and PG-C1, piezometers were installed at the center of the groups, where r of PG-B1 and PG-C1 were 645 mm (r/r_{shaft} = 17.7) and 430 mm (r/r_{shaft} = 11.8), respectively. The u_e time histories of PG-B1 and PB-C1 were used to interpret the behaviour of PG-B2 and PG-C2. It was deemed appropriate to do so because the pile geometry and embedment depth were consistent for all piles and the site was considered relatively homogenous.

Figure 4-13 shows the measured u_e normalized by the initial vertical effective stress (σ'_{v0}) versus the time after the initiation of the pile group installation; the inset figure shows the curves of the first 24 hr and labels the instant when load testing began. The duration of a pile group installation was 0.75 to 1 hr. It is shown that for all piezometers the instantaneous u_e response, during or immediately after pile installation, was negligible. Cavity expansion theory explains that after pile installation there is a region around the pile shaft that is plastically deformed. Within the plastic zone, the instantaneous u_e decreases logarithmically with distance from the pile shaft and reaches zero outside the plastic zone (Randolph and Wroth 1979; Gibson and Anderson 1961). Following Randolph and Wroth (1979), the radius of the plastic zone in the present study was estimated as $10r_{shaft}$ to $14r_{shaft}$, given an estimated G/s_u of 100 to 200 (Duncan and Buchignani 1987), where G is the soil shear modulus. In the present study, the instantaneous u_e was negligible because the piezometers were on the verge of, or outside, the plastic zone ($r/r_{shaft} \geq 11.8$). Further, the low sensitivity of the stiff clay also depressed the generation of u_e (as observed by (Poulos and Davis 1980).

After pile installation, u_e started to increase, which was also predicted by Randolph and Wroth (1979) for soils on the verge of or outside the plastic zone. There was a significant delay (16 to 25 hr) between the initiation of pile installation and measuring a peak u_e. The time lag to the peak u_e was caused by a hydraulic gradient between the piles and the piezometer resulting in a redistribution of u_e away from the piles (Sully and Campanella 1994). The time lag of the peak measured u_e was longer for PG-B1 (25 hr) than for PG-C1 (16 hr) because the r/r_{shaft} ratio was greater for PG-B1. The maximum u_e response of the three tests was measured at PG-C1, where the u_e/σ'_0 ratio reached a peak of 0.288 (u_e = 24.0 kPa), while for PG-B1, the peak measured u_e/σ'_0 ratio was 0.105 (u_e = 8.7 kPa). The higher u_e at PG-C1 was in part due to the closer proximity of the piezometer to the piles for PG-C1 than for PG-B1; also, the smaller s_g of PG-C1 may have caused more overlap in the zones of u_e generation between the grouped piles. The u_e near P-1 was significantly lower than that of the groups. P-1 had a peak u_e/σ'_0 ratio of 0.026 (u_e = 1.9 kPa), occurring 22 hr after pile installation. The magnitude of u_e was much lower for P-1 because there were no compounding effects from multiple piles and because the piezometer for P-1 was located further from the pile toe than PG-B1 and PG-C1.

Figure 4-13 shows that the remaining u_e at t_s of PG-B1 (8 days) was negligible (u_e/σ'_0 = 0.014), and that u_e dissipation was complete at t_s of PG-C1 (9 days). This implies that the soil shear strength had fully recovered when these groups were tested.

The degree of consolidation (U) versus time trend was plotted in Figure 4-14. The value of U was calculated as:

$$U = \frac{u_{max} - u}{u_{max} - u_0} \qquad \text{[Equation 4-10]}$$

where u_{max} is the maximum pore pressure, u_0 is the initial pore pressure, and u (= $u_e + u_0$) is the instantaneous pore pressure. In Figure 4-14, the post-peak time was recorded with respect to the instant when u_{max} was measured. It is shown that initially the measured u_e dissipated fastest for PG-C1. The time to reach 50% consolidation (U_{50}) for PG-C1 was 2170 min, while it was 4415 and 3600 min for PG-B1 and P-1, respectively. However, to reach U_{100}, P-1 was the fastest, at 4.5 days, compared to 7.7 days for PG-C1. PG-B1 was tested before reaching U_{100}; however, based on the measured trend, the time for PG-B1 to reach U_{100} would have been greater than that of PG-C1. In summary, a greater s_g resulted in a longer time to complete u_e dissipation, likely because the drainage path was lengthened.

4.5.6 Effects of Soil Setup on Group Performance

The effects of soil setup on group performance were evaluated by testing PG-B2 and PG-C2 at 5 hr after pile installation and comparing their performance to PG-B1 and PG-C1, which were tested 8 to 9 days after pile installation. Figure 4-11 shows the group efficiencies of these tests. The value of η_g for PG-B2 (s_g/D = 3) was 89.5%, which was a drop of 6.0 percentage points compared to η_g of PG-B1; η_g of PG-C2 (s_g/D = 2) was 78.5%, which was a drop of 12.2 percentage points compared to η_g of PG-C1.

Figure 4-12 shows the R_s versus FS of the tests described above. The values of R_s were consistently higher for the tests performed 5 hr after installation (PG-B2 and PG-C2) compared to the comparable tests performed at least 8 days after installation (PG-B1 and PG-C1). At FS of 1.0, R_s for PG-C2 and PG-C1 were 3.50 and 1.88, respectively, while for PG-B2 and PG-B1, R_s was 2.01 and 1.38, respectively. For all tests, R_s decreased with increasing FS (i.e. decreasing load).

The findings indicate that both group capacity and group settlement were significantly affected by u_e. As s_g decreased, the pore pressure distributions between neighbouring piles overlapped, resulting in a larger cumulative u_e response and larger temporary decrease in shear strength near the piles; thus, resulting in a temporary reduction in η_g and increase in R_s. These findings are corroborated by the measured u_e at the center of PG-B1 and PG-C1 (Figure 4-13).

4.5.7 Failure Mechanism and Load Transfer

The strain gauge data from PG-D1, PG-D2, and P-4 were used to estimate the load distributions along these piles. All piles involved had an s/D ratio of 5 and all group tests had an s_g/D ratio of 2. For all tests, t_s was at least 7 days to allow for complete u_e dissipation. The estimated load distributions were compared to the IBM-predicted (Equation 4-5) distribution to verify the pile failure mechanism. The parameters used in the calculation of the IBM-predicted distribution were: α of 0.3, N_t of 9, and s_u of 65 kPa in the stiff clay and topsoil and 100 kPa in the silty clay crust (Figure 4-3). Figure 4-15 shows the IBM–predicted distribution along with the measured distributions of the instrumented piles, shown at the ultimate state. It appears that the IBM closely predicts the load distribution of the grouped and single piles, as shown by the significant upper-helix bearing resistance and the relatively small inter-helix resistance of these piles. The load distribution of P-4 was similar to that of the piles in PG-D1 and PG-D2; however, for the grouped piles, the lower-helix bearing resistance (Q_{b2}) was larger, and the upper-helix bearing resistance (Q_{b1}) was smaller, than those of P-4. The value of Q_{b1} is shown by the differential load between SG-2 and SG-3, while Q_{b2} is shown by the load measured at SG-4.

To further investigate the pile load transfer, the ratio of the net bearing pressure (q_b) to s_u of both the upper and lower-helices were plotted against pile settlement. Net bearing pressure was calculated by dividing the measured helix resistance (Q_{b1} or Q_{b2}) by the helix bearing area (A_b), where A_b of the lower-helix included the area of the shaft tip. Figure 4-16 shows the measured q_b/s_u trend of the helices of the instrumented piles. At the ultimate state, the measured q_b/s_u ratio is equal to the bearing capacity coefficient N_t, defined in Equation 4-11:

$$N_t = \frac{Q_{b,ult}}{A_b \cdot s_u} \qquad \text{[Equation 4-11]}$$

where $Q_{b,ult}$ is the helix bearing resistance (Q_{b1} or Q_{b2}) measured at the ultimate state.

As shown in Figure 4-16, for the grouped piles, N_t of the lower-helix was greater than that of the upper-helix. For PG-D1 and PG-D2, the measured N_t of the lower-helices were 9.7 and 10.4 respectively, while the upper-helices had N_t of 5.4 and 6.1, respectively. The N_t values of P-4 were 7.0 and 7.7 for the upper and lower-helices, respectively; these values were consistent with those measured during other single pile tests performed by Lanyi and Deng (2017a), who found N_t ranged between 6.2 and 7.7.

For the group tests, N_t of the lower-helices were both greater than a recommended value of 9.0 (Perko 2009; CFEM 2006), while N_t of the upper-helices were significantly less than 9.0. Also, for both the helices of P-4, N_t was below 9.0. These findings indicate that N_t of 9.0 may not be representative of the bearing resistance of helical plates.

4.5.8 Evaluating the Group Failure Mechanism

The validity of the helical pile group block failure model (Perko 2009) was evaluated by comparing the measured Q_{ug} to the predicted Q_{ug} using Equation 4-3. For the predicted Q_{ug}, $q_{b,ult}$ was calculated as $9s_u$ (s_u = 65 kPa) following Perko's (2009) recommendation. Table 4-2 compares the measured and predicted Q_{ug} at various s_g/D ratios, for pile groups with complete u_e dissipation. The block failure model overestimated the group capacity in all cases, and the overestimation increased as the s_g/D ratio increased. This result shows that block failure did not occur for any of these groups.

The load transfer data from PG-D1 and PG-D2 clearly shows that individual pile failure occurred, as significant upper-helix bearing resistance was measured for both tests (Figure 4-15). If block failure had occurred, the differential load between SG-2 and SG-3 should have been much smaller. As PG-D1 and PG-D2 had the lowest s_g/D ratio, it is likely all other pile groups also exhibited individual pile failure, since block failure is less likely at larger s_g/D ratios.

4.6 Conclusions

Field load tests were conducted on seven helical pile groups and four single piles in a relatively homogeneous glaciolacustrine clay. The group pile spacing, inter-helix spacing, and soil setup time were varied among the tests. The following conclusions may be drawn:

1. The group efficiency (η_g) decreased as the s_g/D ratio decreased. The measured η_g of groups with a s_g/D ratio of 2, 3, and 5 were 90.7%, 95.5%, and 96.8%, respectively. The group interaction of helical piles was lower than that predicted for conventional piles at equal s_g/D ratios. The settlement ratio (R_s) increased as the s_g/D ratio decreased. At the group FS of 1.0, R_s was 1.88, 1.38, and 1.26 for groups with a s_g/D ratio of 2, 3, and 5, respectively; group interaction increased with increasing group load.
2. The instantaneous installation-induced u_e was negligible at the center of pile groups with s_g/D ratios of 2 and 3 (r/r_{shaft} = 11.8 and 17.7, respectively) and near the single pile (r/r_{shaft} = 12.3). After installation, u_e increased as pore pressure redistributed away from the piles.
3. The magnitude of u_e at the center of groups increased, and the time to reach U_{100} was shortened, as the s_g/D ratio decreased. At the center of the groups, the magnitude of u_e and the time to reach U_{100} exceeded those measured near the single pile.
4. Group performance was significantly affected by installation-induced u_e. Groups with s_g/D ratios of 2 and 3, which were tested at t_s of 5 hr, had significantly decreased η_g and increased R_s, when compared to groups tested at t_s of 8 to 9 days. This reduction in group performance increased as the s_g/D ratio decreased.
5. Single piles and pile groups (s_g/D = 2) containing piles with an s/D ratio of 5 exhibited individual bearing failure. The grouped piles had more load resisted by the lower-helix and less load resisted by the upper-helix compared to that of an equivalent single pile. For the group tests, the measured N_t was 5.8 for the upper-helix and 10.1 for the lower-helix, on average. For the single pile, N_t was 7.0 and 7.7 for the upper and lower helices, respectively.

6. The block failure model heavily overestimated the capacities of all test groups. Load distributions of the instrumented piles in PG-D1 and PG-D2 clearly showed that individual pile failure occurred. All other groups likely exhibited individual pile failure as well.

Table 4-1. Load test description and results.

	Test ID	t_s	s/D	s_g/D	Q_u (kN)	K_t (m^{-1})	Instrumentation
Pile Groups	PG-A1	7 day	3	5	401.6	N/A	N/A
	PG-B1	8 day	3	3	450.3	N/A	Piezometer PZ-2
	PG-B2	5 hr	3	3	381.9	N/A	N/A
	PG-C1	9 day	3	2	507.8	N/A	Piezometer PZ-3
	PG-C2	5 hr	3	2	371.0	N/A	N/A
	PG-D1[a]	8 day	5	2	N/A	N/A	Strain Gauges
	PG-D2[a]	7 day	5	2	N/A	N/A	Strain Gauges
Single Piles	P-1[b]	6 day	3	N/A	N/A	N/A	Piezometer PZ-1
	P-2	15 day	3	N/A	101.5	23.4	N/A
	P-3	12 day	3	N/A	89.3	23.9	N/A
	P-4	18 day	5	N/A	93.9	22.8	Strain Gauges

Note: (*a*) Load test stopped prior to reaching Q_u due to severe differential settlement; (*b*) Load test without pile rotation constraint on the pile cap.

Table 4-2. Comparison of measured group capacities and block failure model predicted capacities.

Test ID	s_g/D	Measured Q_{ug} (kN)	Predicted Q_{ug} (kN)	$\frac{\text{Measured } Q_{ug}}{\text{Predicted } Q_{ug}}$
PG-A1	5	402	2391	16.8%
PG-B1	3	450	1159	38.8%
PG-C1	2	508	707	71.9%

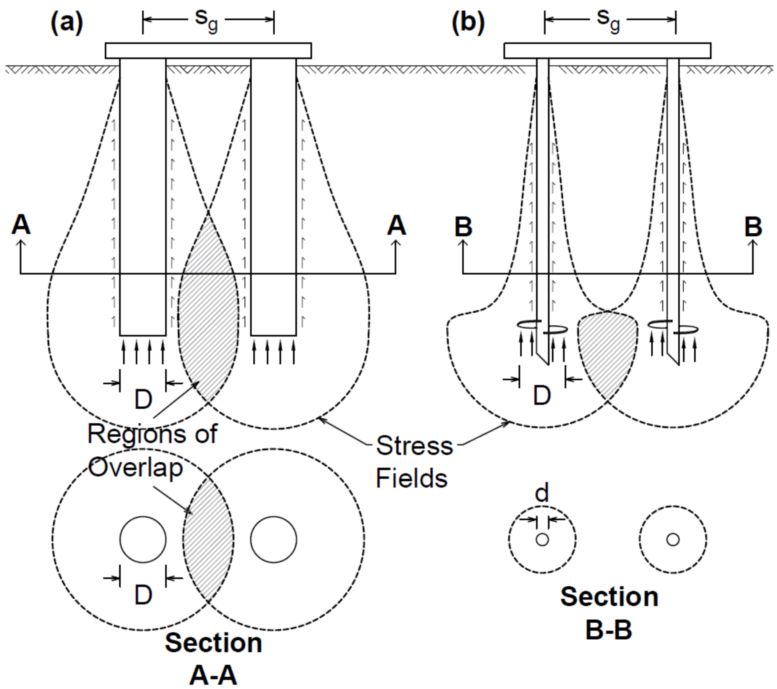

Figure 4-1. Conceptual schematic of stress fields around pile groups: (a) conventional pile group (adapted from Bowles 1997 and Hannigan et al. 2016); and (b) helical pile group.

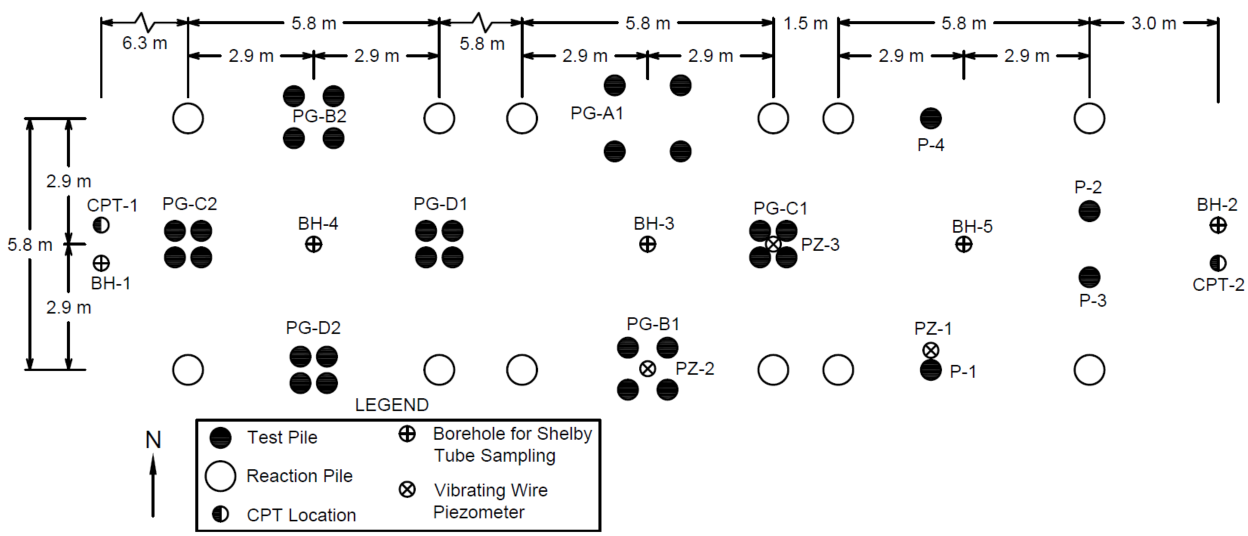

Figure 4-2. Test site layout and site investigation activities. Test site location: Edmonton, Alberta (53°29’54” N, 113°31’57” W).

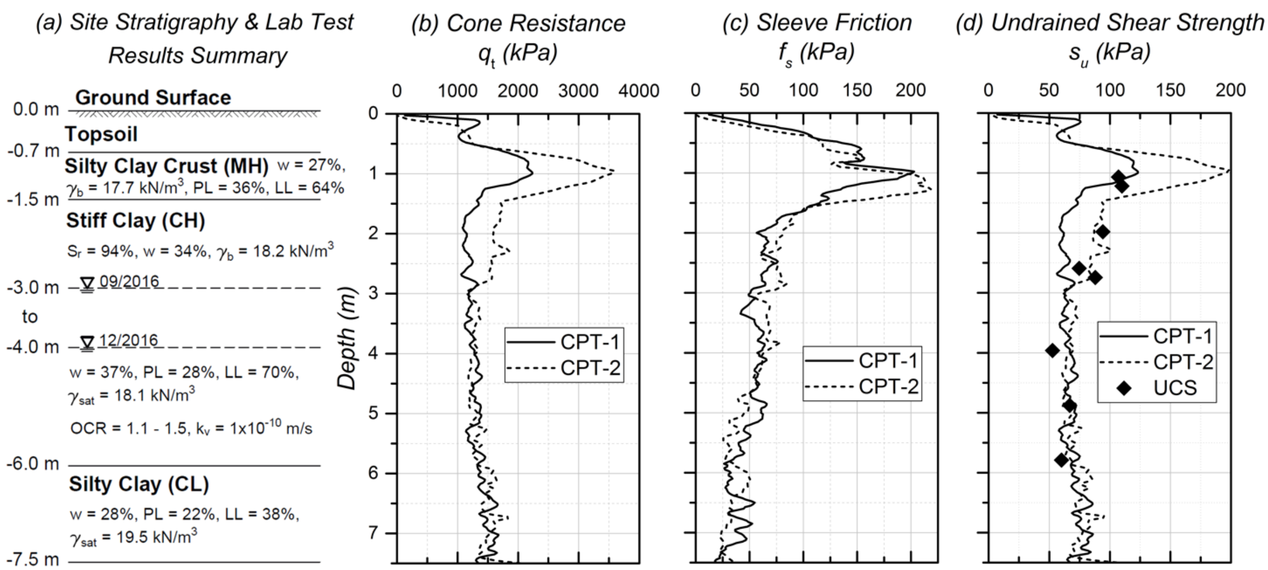

Figure 4-3. (a) Site stratigraphy and lab test results summary; (b) CPT cone resistance profile; (c) CPT sleeve friction profile; and (d) undrained shear strength profile.

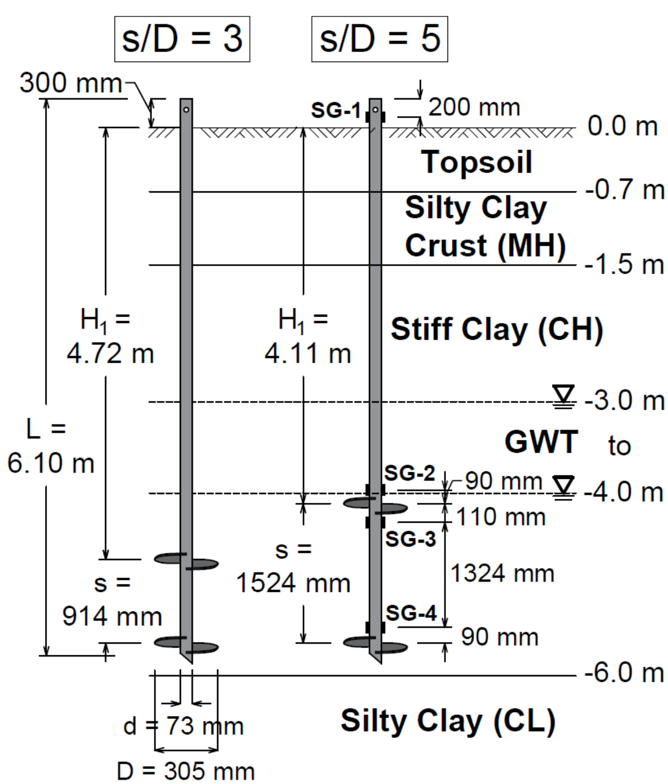

Figure 4-4. Test pile schematic with dimensions and strain gauge locations. Note: *L*, *d*, and *D* are equal for all test piles.

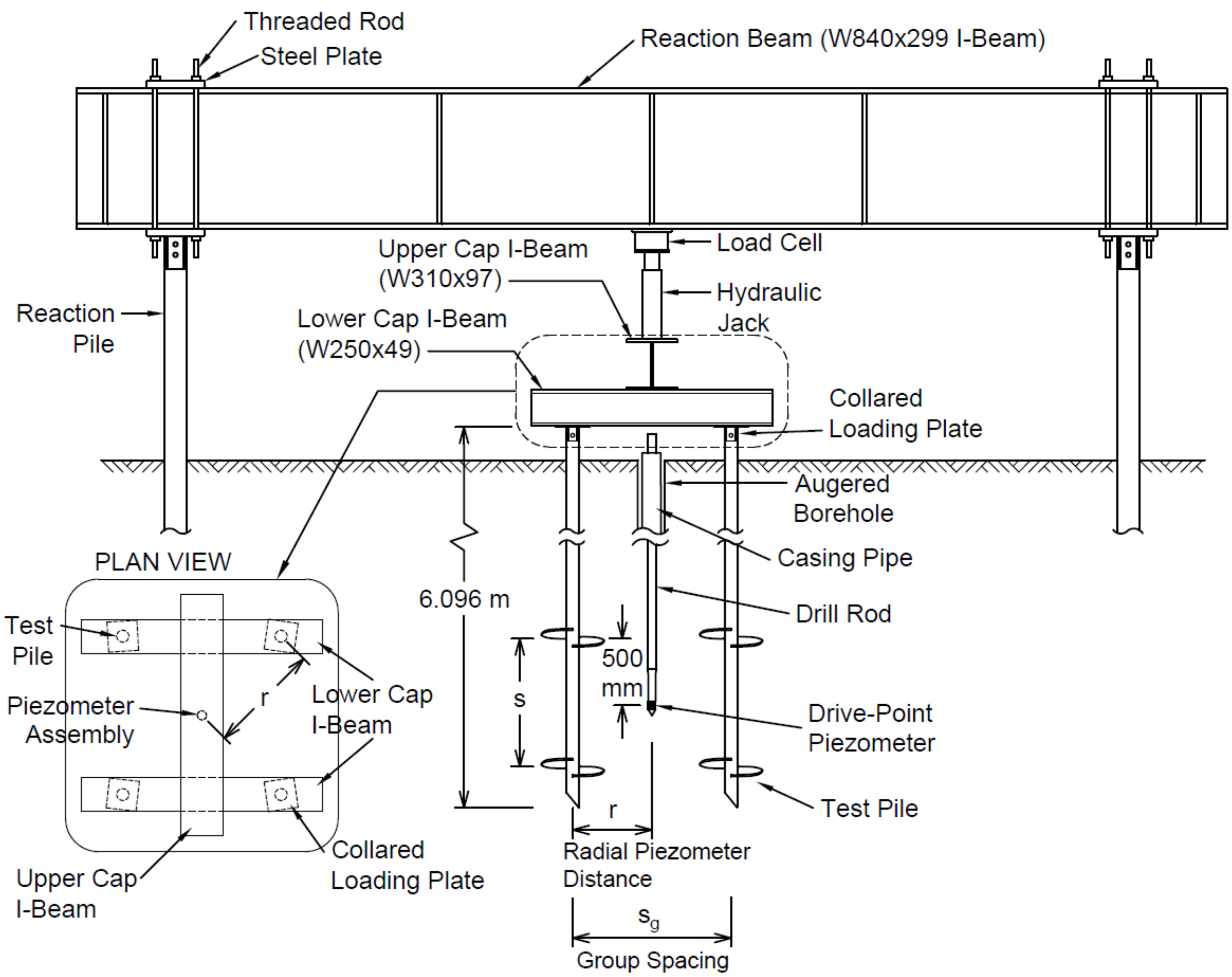

Figure 4-5. Pile group load test setup and piezometer assembly schematic. Note: piezometer installation for group tests PG-B1 and PG-C1 only. Same setup was used for single pile tests except that the group cap assembly was not required.

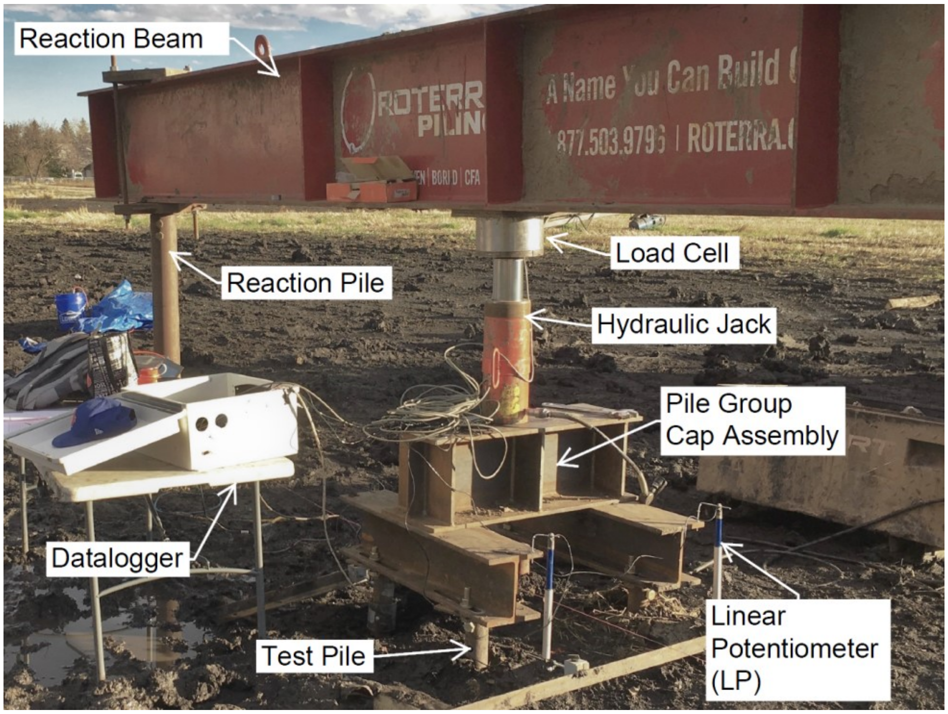

Figure 4-6. Photo of a typical pile group test.

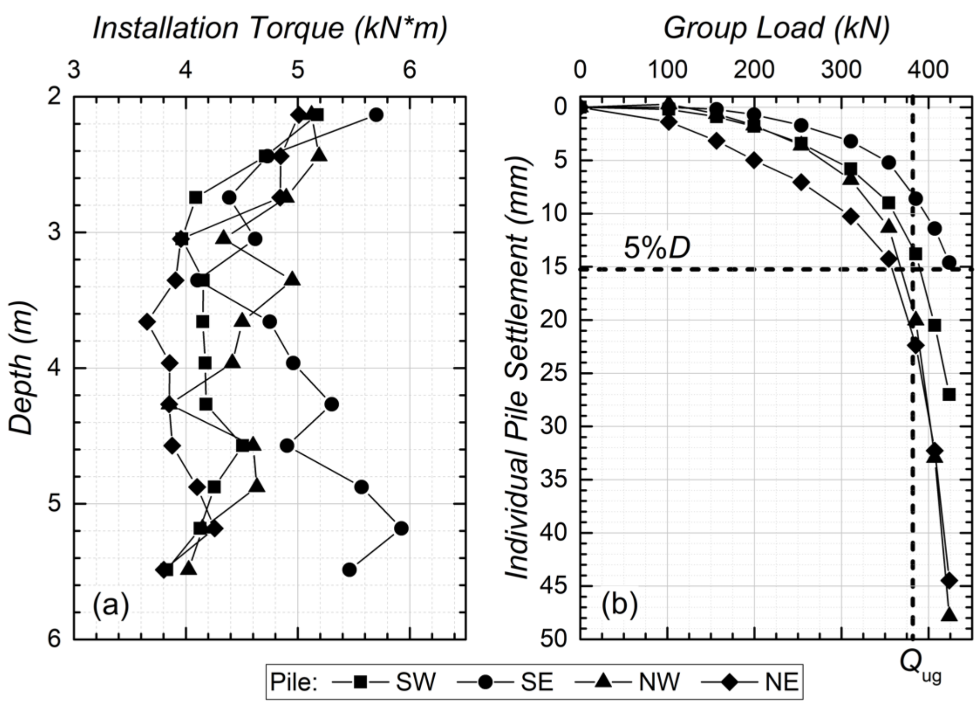

Figure 4-7. (a) PG-B2 installation torque profiles; and (b) PG-B2 pile group load vs. individual pile settlement curves.

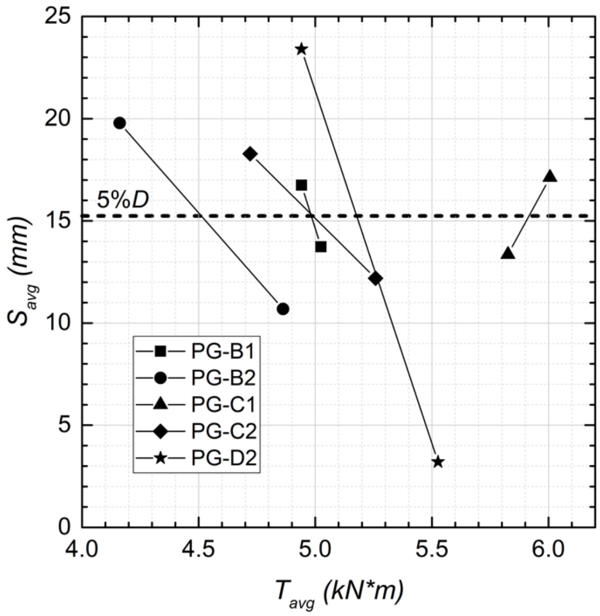

Figure 4-8. Pile group average torque (T_{avg}) versus average settlement (S_{avg}). T_{avg} and S_{avg} are the average T and S, respectively, of two piles in a rigidly connected set under the same lower-cap I-beam, where S_{avg} is measured at the ultimate state.

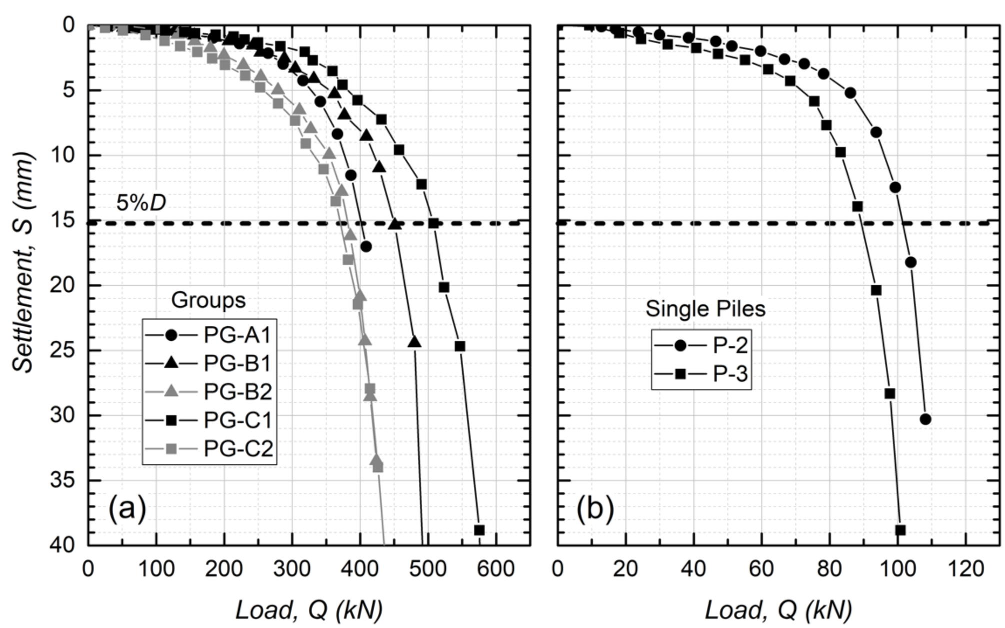

Figure 4-9. (a) Pile group load – settlement curves; (b) single pile load – settlement curves.

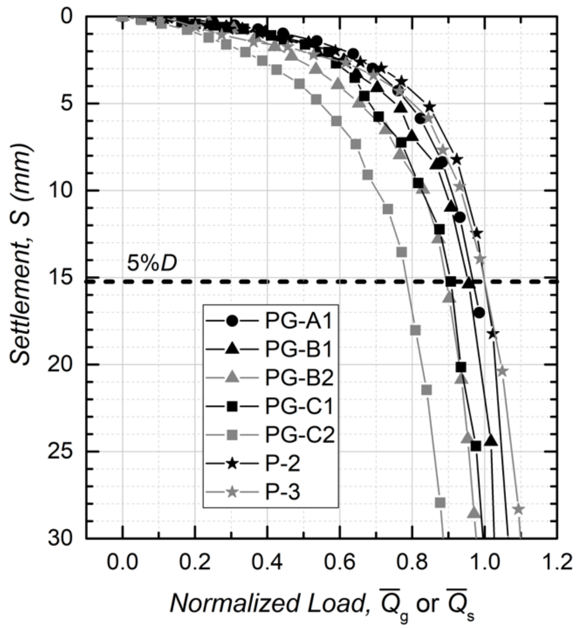

Figure 4-10. Pile group and single pile normalized load – settlement curves.

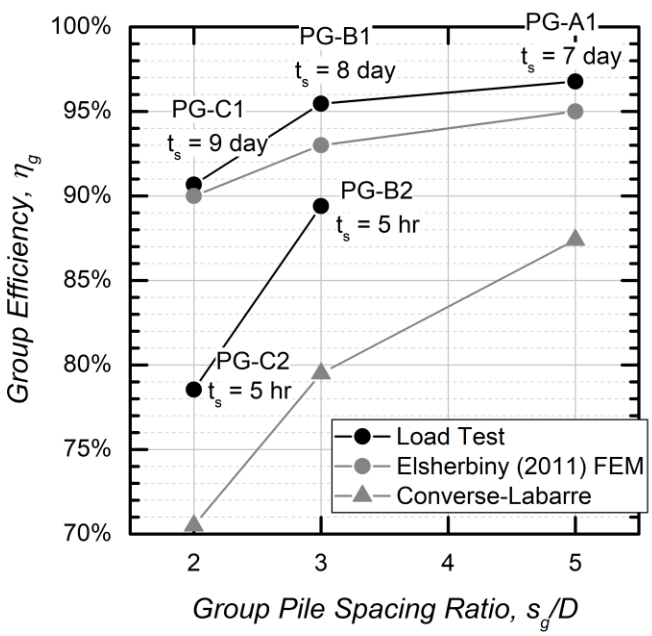

Figure 4-11. Group efficiency vs. group pile spacing ratio. Key parameters in Elsherbiny (2011): Q_u at S = 5%D, s_u = 75 kPa, L = 6.2 m, d = 273 mm, D = 610 mm, n = 2, s/D = 3, and 2×2 group.

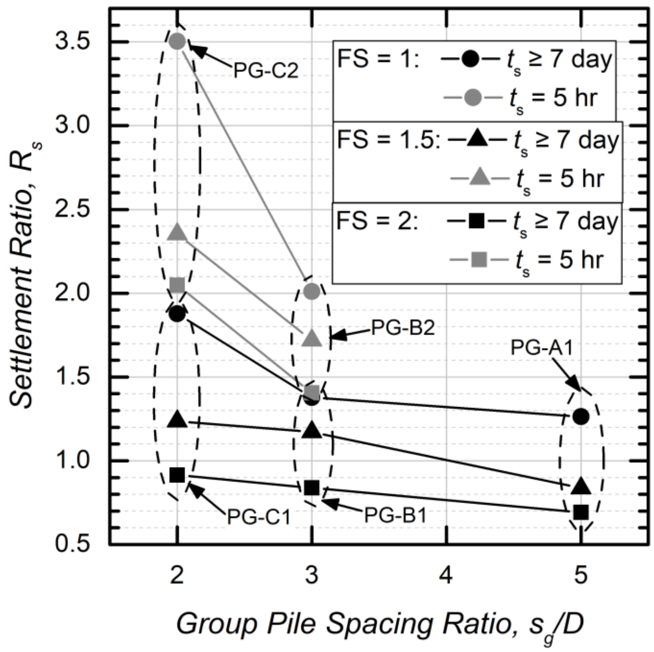

Figure 4-12. Settlement ratio vs. group pile spacing ratio at selected pile group FS.

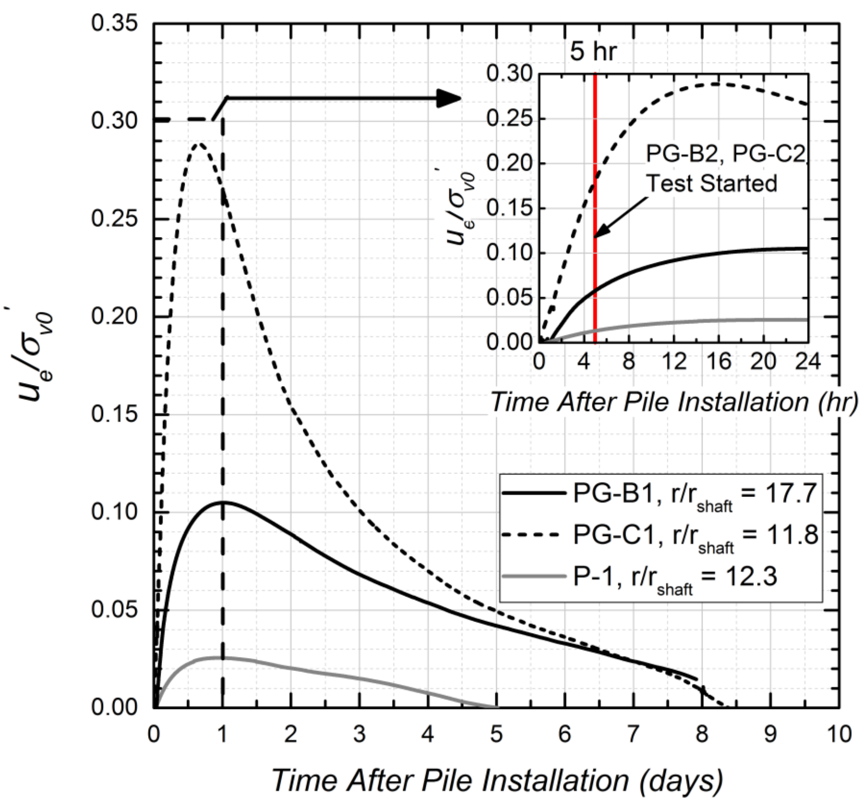

Figure 4-13. Installation-induced pore pressure generation and dissipation for tests PG-B1, PG-C1, and P-1.

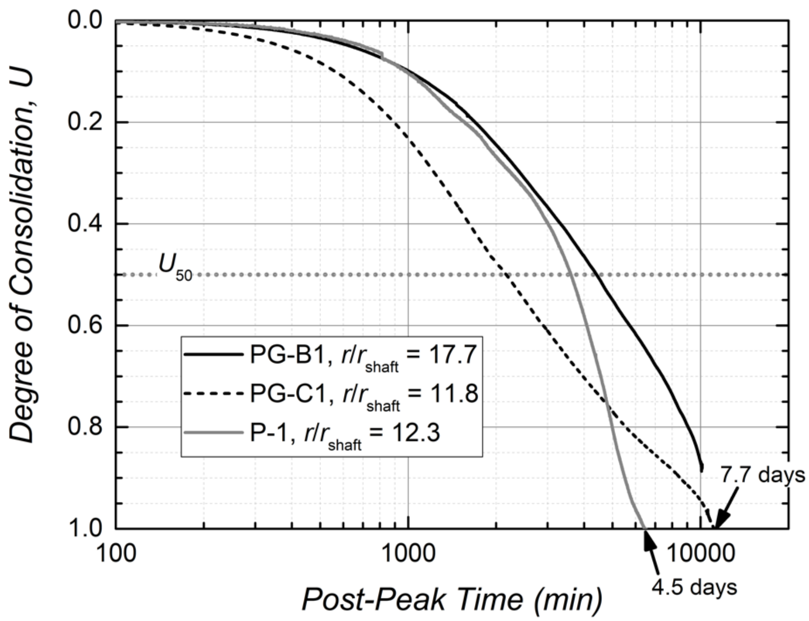

Figure 4-14. Degree of consolidation vs. post-peak time for tests PG-B1, PG-C1, and P-1.

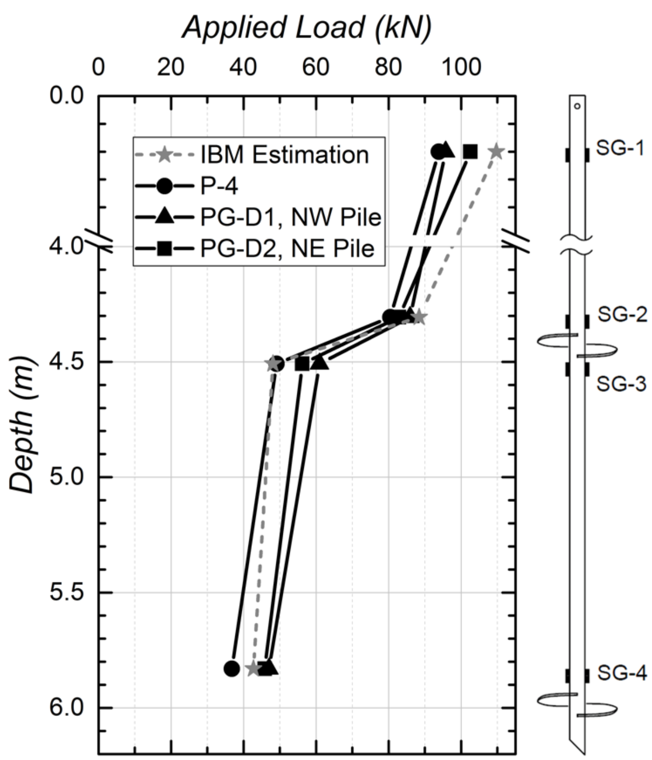

Figure 4-15. Measured pile load distributions for piles with *s/D* of 5, at the ultimate state.

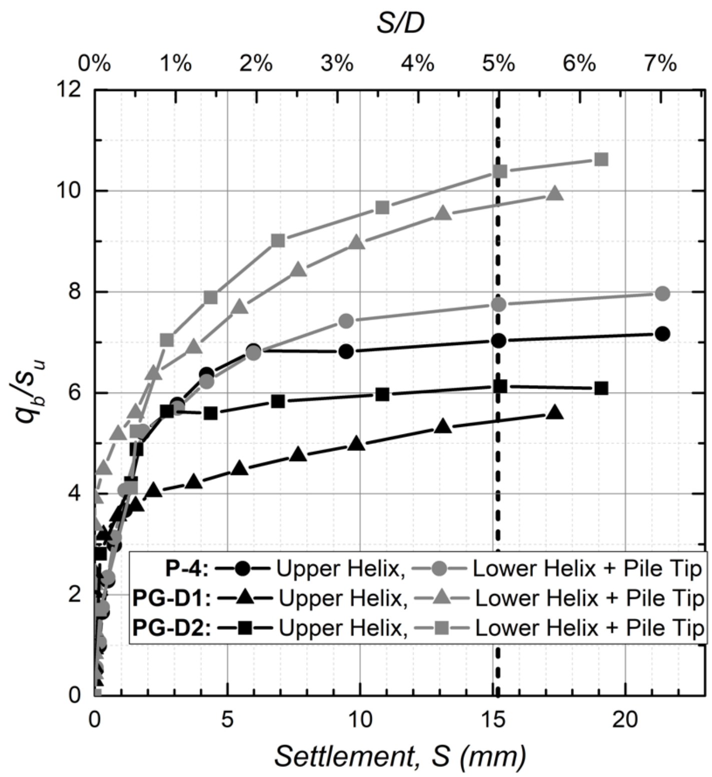

Figure 4-16. Development of helix net bearing pressure normalized by soil undrained shear strength.

5 Conclusions and Recommendations

5.1 Summary and Conclusions

Full-scale field load tests were conducted on single and grouped helical piles at a cohesive soil site in Edmonton, Alberta. All single test piles were instrumented with strain gauges; their inter-helix spacing ratios (*s/D*) were varied at 1.5, 3, and 5. Pile groups had a 2 × 2 configuration with varied center-to-center pile spacing (s_g) to helix diameter (*D*) ratios (s_g/D = 2, 3, 5). Selected pile groups contained a test pile with strain gauge instrumentation. For both single pile and group tests, the time between pile installation and testing varied between comparable piles or groups. One set of tests was conducted shortly after pile installation (2 to 5 hr), while another set was conducted at least 7 days after installation. Piezometers were installed at the center of selected pile groups and near a single test pile in order to measure the excess pore pressure response to pile installation and monitor the rate of dissipation. The following conclusions can be drawn.

5.1.1 Axial Behaviour of Single Helical Piles in a Cohesive Soil

1. In the homogeneous stiff cohesive soil (s_u = 65 kPa), the individual bearing model dominated pile behaviour at the ultimate state. Piles with *s/D* ratios of 1.5, 3, and 5 had measured cylindrical shear resistances far below the cylindrical shear model predicted resistance and had helix bearing resistances closely predicted by the individual bearing model.
2. A model is proposed to describe the transition from individual bearing behaviour to cylindrical shear behaviour. This process involves the progressive growth of a soil cylinder under the upper-helix. As the pile load increases the soil cylinder extends toward the lower-helix. The bearing resistance of the upper-helix begins to decline when the lower-helix begins to obstruct the mobilized shear resistance of the upper-helix bearing.

3. Helical pile load transfer behaviour in cohesive soils is not only dependent on the inter-helix spacing ratio, but also the soil strength and pile load. It is more likely for a larger soil cylinder to develop, and the cylindrical shear model to dominate pile behaviour, in less stiff soils. This is because less force is required to mobilize shearing along the cylindrical surface.
4. The measured bearing capacity coefficient (N_t) for the helical plates was between 6.2 and 7.7 at the ultimate pile load, which is substantially lower than the commonly used value of 9. The low measured N_t values are likely due to the inclination of the helical plate bearing surface. Helical plate bearing resistance was found to fully mobilize after a pile settlement of 15 to 20 mm (5% to 6.6%D).
5. The measured shaft resistance (Q_s) of most the test piles reached a peak after 2 to 4 mm (3% to 5.5%d) of pile settlement. The peak shaft adhesion factors (α) of these piles were between 0.11 and 0.14. At plunging failure, the measured α of these piles were between 0.06 and 0.10.
6. Installation-induced u_e caused a temporary resistance reduction to a pile tested 2 hours after installation (PA-4). At low settlement, the resistance ratio (R_r) of PA-4 with respect to PA-2 and PA-3 was 0.75; however, as the pile was loaded to its ultimate capacity, R_r approached unity. The increased settlement caused the bearing failure of the helical plates to mobilize soil shear resistance further from the pile where u_e generation was negligible.

5.1.2 Axial Behaviour of Helical Pile Groups in a Cohesive Soil

1. The group efficiency (η_g) decreased as the s_g/D ratio decreased. The measured η_g of groups with a s_g/D ratio of 2, 3, and 5 were 90.7%, 95.5%, and 96.8%, respectively. The group interaction of helical piles was lower than that predicted for conventional piles at equal s_g/D ratios. The settlement ratio (R_s) increased as the s_g/D ratio decreased. At the group FS of 1.0,

R_s was 1.88, 1.38, and 1.26 for groups with a s_g/D ratio of 2, 3, and 5, respectively; group interaction increased with increasing group load.

2. The instantaneous installation-induced u_e was negligible at the center of pile groups with s_g/D ratios of 2 and 3 (r/r_{shaft} = 11.8 and 17.7, respectively) and near the single pile (r/r_{shaft} = 12.3). After installation, u_e increased as pore pressure redistributed away from the piles.
3. The magnitude of u_e at the center of groups increased, and the time to reach U_{100} was shortened, as the s_g/D ratio decreased. At the center of the groups, the magnitude of u_e and the time to reach U_{100} exceeded those measured near the single pile.
4. Group performance was significantly affected by installation-induced u_e. Groups with s_g/D ratios of 2 and 3, which were tested at t_s of 5 hr, had significantly decreased η_g and increased R_s, when compared to groups tested at t_s of 8 to 9 days. This reduction in group performance increased as the s_g/D ratio decreased.
5. Single piles and pile groups (s_g/D = 2) containing piles with an s/D ratio of 5 exhibited individual bearing failure. The grouped piles had more load resisted by the lower-helix and less load resisted by the upper-helix compared to that of an equivalent single pile. For the group tests, the measured N_t was 5.8 for the upper-helix and 10.1 for the lower-helix, on average. For the single pile, N_t was 7.0 and 7.7 for the upper and lower helices, respectively.
6. The block failure model heavily overestimated the capacities of all test groups. Load distributions of the instrumented piles in PG-D1 and PG-D2 clearly showed that individual pile failure occurred. All other groups likely exhibited individual pile failure as well.

5.2 Recommendations for Further Research

The current investigation on single helical pile behaviour was limited in that all piles tests occurred in a relatively homogeneous soil that had a low sensitivity. To further investigate the influence of soil stiffness on pile load transfer, testing could be performed at several cohesive soil sites with a wide range of soil shear strengths or sensitivities. Also, in order to obtain better resolution of the pile load distributions, test piles could be instrumented with more strain gauges in the inter-helix zone and on the upper-shaft. This could lead to a better understanding of the development of cylindrical shear and shaft resistance.

The current study is one of the first to investigate the group behaviour of helical piles through full-scale field testing, and as such, there are many opportunities to further this area of study. The current study investigated the behaviour of 2 × 2 helical pile groups in a stiff clay under axial compressive loading. Possible permutations of this study include: varying the group configuration and the number of piles in a group, testing groups in cohesionless soil, testing piles fixed to a rigid pile cap, and testing groups under tensile or lateral loads. Improved instrumentation, particularly strain gauges instrumented grouped piles, would be desired in order to determine the load transfer and failure mechanism in pile groups.

In the current study, the installation-induced u_e was measured at only one location for single pile or pile group tests. To better understand the distribution of u_e generation and the rate of u_e dissipation, u_e could be measured at various radial distances away from the piles and at various depths. More piezometer records could verify whether the radial consolidation theory and the cavity expansion theory predict the pore pressure generation around a helical pile. Additionally, the effects of u_e on the short-term single pile and pile group performance could be further investigated by performing tests at many different setup times. Lastly, testing of groups could occur in a highly sensitive soil, as greater u_e generation would be expected.

References

Adams, J. I., and Klym, T. W. (1972). "A study of anchorages for transmission tower foundations." *Can. Geotech. J.,* 9 89-104.

ASCE. (1993). "Bearing Capacity of Soils." *Technical Engineering and Design Guides as Adapted from U.S. Army Corps of Engineers, No. 7,* ASCE Press, New York, NY.

ASTM D1143M-07. (2007). *Standard test methods for deep foundations under axial compressive load.* ASTM International, West Conshohocken, PA.

Bayrock, L. A., and Hughes, G. M. (1962). "Surficial Geology of the Edmonton District, Alberta." *Rep. No. Preliminary Report 62-6,* Research Council of Alberta, Edmonton, AB.

Bolin, H. W. (1941). "The pile efficiency formula of the Uniform Building Code." *Building Standards Monthly,* 10(1), 4-5.

Bowles, J. E. (1997). *Foundation Analysis and Design, 5th ed.* McGraw-Hill, Singapore.

Carville, C. A., and Walton, R. W. (1995). "Foundation repair using helical screw anchors." *Foundation Upgrading and Repair for Infrastructure Improvement, ASCE,* 56-75.

CFEM. (2006). *Canadian Foundation Engineering Manual. 4th ed.* Canadian Geotechnical Society, BiTech Publisher Ltd., Canada.

Duncan, J. M., and Buchignani, A. L. (1987). *Engineering Manual for Settlement Studies.* Virginia Tech, Blacksburg, VA.

El Naggar, M. H., and Abdelghany, Y. (2007). "Helical screw piles (HSP) capacity for axial cyclical loadings in cohesive soils." *4th International Conference on Earthquake Geotechnical Engineering,* Thessaloniki, Greece.

Elkasabgy, M., and El Naggar, M. H. (2015). "Axial compressive response of large-capacity helical and driven steel piles in cohesive soil." *Can. Geotech. J.,* 52 224-243.

Elsherbiny, Z. (2011). "Axial and lateral performance of helical pile groups". Master's Thesis. University of Western Ontario, London, ON.

Elsherbiny, Z., and El Naggar, M. H. (2013). "Axial compressive capacity of helical piles from field tests and numerical study." *Can. Geotech. J.,* 50 1191-1203.

Fellenius, B. H. (1999). "Bearing capacity of footings and piles - a delusion?" *DFI Annual Meeting,* Dearborn, MI.

Fleming, K., Weltman, A., Randolph, M. F., and Elson, K. (2009). *Piling Engineering, 3rd ed.* Taylor & Francis, London and New York.

Ghaly, A., and Hanna, A. (1994). "Model investigation of the performance of single anchors and groups of anchors." *Can. Geotech. J.,* 31 273-284.

Gibson, R. E., and Anderson, W. F. (1961). "In situ measurement of soil properties with the pressuremeter." *Civil Engineering and Public Works Review,* 56(658), 615-618.

Godfrey, J. D. (1993). *Edmonton Beneath our Feet: a Guide to the Geology of the Edmonton Region.* Edmonton Geological Society, Edmonton, AB.

Hanna, A. M., Morcous, G., and Helmy, M. (2004). "Efficiency of pile groups installed in cohesionless soil using artificial neural networks." *Can. Geotech. J.,* 41 1241-1249.

Hannigan, P. J., Rausche, F., Likins, G. E., Robinson, B. R., and Becker, M. L. (2016). "Geotechnical Engineering Circular No. 12 – Volume I, Design and Construction of Driven Pile Foundations." *Rep. No. FHWA-NHI-16-009,* USDOT, D.C.

Hoyt, R. M., and Clemence, S. P. (1989). "Uplift capacity of helical anchors in soil." *12th International Conference on Soil Mechanics and Foundation Engineering,* Rio de Janeiro, Brazil, 1019-1022.

Hu, Y., and Randolph, M. F. (2002). "Bearing capacity of caisson foundations on normally consolidated clay." *Soils and Foundations,* 42(5), 71-77.

Lanyi, S. A., and Deng, L. (2017a). "Effects of inter-helix spacing and soil setup on the behaviour of axially loaded helical piles in cohesive soil." *Soils and Foundations,* (in review).

Lanyi, S. A., and Deng, L. (2017b). "Axial load testing of helical pile groups in a glaciolacustrine clay." *Can. Geotech. J.,* (in review).

Lee, S., and Chung, C. (2005). "An experimental study of the interaction of vertically loaded pile groups in sand." *Can. Geotech. J.,* 42 1485-1493.

Livneh, B., and El Naggar, M. H. (2008). "Axial testing and numerical modelling of square shaft helical piles under compressive and tensile loading." *Can. Geotech. J.,* 45 1142-1155.

Lutenegger, A., Erikson, J., and Williams, N. (2014). "Evaluating installation disturbance of helical anchors in clay from field vane tests." *Proceedings of the 39th Annual Conference on Deep Foundations,* Atlanta, GA.

Lutenegger, A. J. (2013). "Underpinning a residential structure on uncontrolled fill with helical screw-piles." *7th International Conference on Case Histories in Geotechnical Engineering,* Chicago, IL.

Lutenegger, A. J. (2011). "Historical development of iron screw-pile foundations: 1836–1900." *Int. J. for the History of Eng. & Tech.,* 81(1), 108-128.

Lutenegger, A. J. (2009). "Cylindrical shear or plate bearing? – uplift behavior of multi-helix screw anchors in clay." *2009 International Foundation Congress and Equipment Expo, Contemporary Topics in Deep Foundations.* ASCE, 456-463.

Lutenegger, A. J., and Tsuha, C. H. C. (2015). "Evaluating installation disturbance from helical piles and anchors using compression and tension tests." *15th Pan-American Conference on Soil Mechanics and Geotechnical Engineering,* Buenos Aires, Argentina.

McCabe, B. A., and Lehane, B. M. (2006). "Behavior of axially loaded pile groups driven in clayey silt." *J. Geotech. Geoenviron. Eng.,* 132(3), 401-410.

Mendoza, C. C., Cunha, R., and Lizcano, A. (2015). "Mechanical and numerical behavior of groups of screw (type) piles founded in a tropical soil of the Midwestern Brazil." *Comput.Geotech.,* 67 187-203.

Meyerhof, G. G. (1960). "The design of franki piles with special reference to groups in sands." *Symposium on Pile Foundations, 6th Congress Int. Assoc. Bridge and Struct. Eng.* Stockholm, Sweden.

Meyerhof, G. G. (1951). "The ultimate bearing capacity of foundations." *Geotechnique,* 2(4), 301-332.

O'Neill, M. W., and Reese, L. C. (1999). "Drilled Shafts: Construction Procedure and Design Methods." *Rep. No. IF-99-025,* FHWA, USDOT, D.C.

Perko, H. A. (2000). "Energy method for predicting installation torque of helical foundations and anchors." *Geo-Denver (ASCE),* Denver, CO.

Perko, H. A. (2009). *Helical Piles: a Practical Guide to Design and Installation.* J. Wiley, Hoboken, N.J.

Perlow, M. (2011). "Evolution of helical screw pile design and installation." *Deep Foundations Institute,* 425-432.

Poulos, H. G. (1989). "Pile behaviour - theory and application." *Geotechnique,* 39(3), 365-415.

Poulos, H. G. (1968). "Analysis of the settlement of pile groups." *Geotechnique,* 18 449-471.

Poulos, H. G., and Davis, E. H. (1980). *Pile Foundation Analysis and Design.* Wiley, New York.

Randolph, M. F. (2003). "Science and empiricism in pile foundation design." *Geotechnique,* 53(10), 847-875.

Randolph, M. F., and Murphy, B. S. (1985). "Shaft capacity of driven piles in clay." *Offshore Technology Conference,* Houston, TX.

Randolph, M. F., and Wroth, C. P. (1979). "An analytical solution for the consolidation around a driven pile." *Int. J. Numer. Anal. Methods Geomech.,* 3 217-229.

Rao, N. S., and Prasad, Y. V. S. N. (1993). "Estimation of uplift capacity of helical anchors in clays." *J. Geotech. Eng.,* 119(2), 352-357.

Rao, N. S., Prasad, Y. V. S. N., Shetty, M. D., and Joshi, V. V. (1989). "Uplift capacity of screw pile anchors." *Journal of Southeast Asian Geotechnical Society,* 20(2), 139-159.

Rao, N. S., Prasad, Y. V. S. N., and Veeresh, C. (1993). "Behaviour of embedded model screw anchors in soft clays." *Geotechnique,* 43(4), 605-614.

Rao, S. N., Prasad, Y. V. S. N., and Shetty, M. D. (1991). "Behaviour of model screw piles in cohesive soils." *Soils and Foundations,* 31(2), 35-50.

Robertson, P. K., and Cabal, K. L. (2015). *Guide to Cone Penetration Testing for Geotechnical Engineering.* Gregg Drilling & Testing, Inc., Signal Hill, CA.

Salgado, R. (2008). *The Engineering of Foundations.* McGraw-Hill, New York.

Shaheen, W. A., and Demars, K. R. (1995). "Interaction of multiple helical earth anchors embedded in granular soil." *Marine Georesources and Geotechnology,* 13(4), 357-374.

Simonsen, T. R., and Sorensen, K. K. (2016). "Field measurements of pore water pressure changes in very high plasticity stiff clays adjacent to driven piles." *17th Nordic Geotechnical Meeting: Challenges in Nordic Geotechnic,* Reykjavik, Iceland.

Skempton, A. W. (1951). "The bearing capacity of clays." *Proceedings of the Building Research Congress,* 180-189.

Skempton, A. W. (1950). "Discussion on: The bearing capacity of screw piles and screwcrete cylinders." *Journal of the Institution of Civil Engineers,* 34(5), 74-93.

Soderberg, L. O. (1962). "Consolidation theory applied to foundation pile time effects." *Geotechnique,* 12(3), 217-225.

Sully, J. P., and Campanella, R. G. (1994). "Evaluation of field CPTU dissipation data in overconsolidated fine-grained soils." *13th International Conference on Soil Mechanics and Foundation Engineering,* New Delhi, 201-204.

Tappenden, K. M. (2007). "Predicting the Axial Capacity of Screw Piles Installed in Western Canadian Soils". Master's Thesis. University of Alberta, Edmonton, AB.

Tappenden, K., Sego, D., and Robertson, P. (2009). "Load transfer behavior of full-scale instrumented screw anchors." *Contemporary Topics in Deep Foundations - 2009 International Foundation Congress and Equipment Expo,* American Society of Civil Engineers, Orlando, FL, 472-479.

Terzaghi, K. (1943). *Theoretical Soil Mechanics.* John Wiley & Sons, Inc., New York.

Trofirnenkov, J. G., and Mariupolskii, L. G. (1965). "Screw piles used for mast and tower foundations." *Proceedings of Sixth lnternational Conference on Soil Mechanics and Foundation Engineering,* Montreal, QC, 328-332.

Vesic, A. S. (1973). "Analysis of ultimate loads of shallow foundations." *Journal of Soil Mechanics and Foundations Division,* 99(SM1), 45-73.

Vyazmensky, A. M. (2005). "Numerical Modelling of Time Dependent Pore Pressure Response Induced by Helical Pile Installation". MSc. University of British Columbia, Vancouver, BC.

Weech, C. (2002). "Installation and Load Testing of Helical Piles in a Sensitive Fine-Grained Soil". Master's Thesis. University of British Columbia, Vancouver, BC.

Weech, C., and Howie, J. (2012). "Helical piles in soft sensitive soils – a field study of disturbance effects on pile capacity." *20th Symposium on Soft Ground Engineering,* Vancouver, BC.

Whitaker, T. (1957). "Experiments with model piles in groups." *Geotechnique,* 7(4), 147-167.

Zhang, D. (1999). "Predicting Capacity of Helical Screw Piles in Alberta Soils". Master's Thesis. University of Alberta, Edmonton, AB.